Biological evaluation of new nickel(II) metallates: Synthesis, DNA/protein binding and mitochondrial mediated apoptosis in human lung cancer cells (A549) via ROS hypergeneration an...

ARTICLE *in* EUROPEAN JOURNAL OF MEDICINAL CHEMISTRY · JUNE 2014

Impact Factor: 3.45 · DOI: 10.1016/j.ejmech.2014.05.075 · Source: PubMed

7 AUTHORS, INCLUDING:

Poornima Paramasivan
Bangor University
26 PUBLICATIONS **300** CITATIONS
SEE PROFILE

Frédéric Dallemer
Aix-Marseille Université
34 PUBLICATIONS **479** CITATIONS
SEE PROFILE

Viswanadha Vijaya Padma
Bharathiar University
76 PUBLICATIONS **548** CITATIONS
SEE PROFILE

Karuppannan Natarajan
Bharathiar University
210 PUBLICATIONS **4,731** CITATIONS
SEE PROFILE

European Journal of Medicinal Chemistry 82 (2014) 584–599

Contents lists available at ScienceDirect

European Journal of Medicinal Chemistry

journal homepage: http://www.elsevier.com/locate/ejmech

Original article

Biological evaluation of new nickel(II) metallates: Synthesis, DNA/protein binding and mitochondrial mediated apoptosis in human lung cancer cells (A549) via ROS hypergeneration and depletion of cellular antioxidant pool

P. Kalaivani [a], S. Saranya [b], P. Poornima [b], R. Prabhakaran [a, *], F. Dallemer [c], V. Vijaya Padma [b], K. Natarajan [a, *]

[a] Department of Chemistry, Bharathiar University, Coimbatore 641 046, India
[b] Department of Biotechnology, Bharathiar University, Coimbatore 641 046, India
[c] Aix Marseille Université, CNRS, MADIREL UMR 7246, 13397, Marseille, France

ARTICLE INFO

Article history:
Received 17 February 2014
Received in revised form
27 May 2014
Accepted 31 May 2014
Available online 3 June 2014

Keywords:
Nickel(II) thiosemicarbazone complexes
CT-DNA/BSA binding
Cytotoxicity
ROS-hypergeneration
Mitochondrial-membrane potential
Depletion of cellular antioxidant pool

ABSTRACT

A series of novel nickel(II) thiosemicarbazone complexes(**1**–**4**) have been prepared and characterized by various spectral, analytical techniques and X-ray crystallography. Further, their efficacy to interact with CT-DNA/BSA has been explored. From the binding studies, it is inferred that complex **4** found to be more active than other complexes. The complexes bound with CT-DNA by intercalation mode. Moreover, static quenching was observed for their interaction with BSA. The new complexes were tested for their *in vitro* cytotoxicity against human lung adenocarcinoma (A549) cell line. The results showed that the new complexes exhibited significant degree of cytotoxicity at given experimental condition. Further, the results of LDH and NO release supported the cytotoxic nature of the complexes. The observed cytotoxicity of the complexes may be routed through ROS-hypergeneration and lipid-peroxidation with subsequent depletion of cellular antioxidant pool (GSH, SOD, CAT, GPx and GST) resulted in the reduction of mitochondrial-membrane potential, caspase-3 activation and DNA fragmentation. Thus, the data from the present study disclose that the complexes could induce apoptosis in A549 cells through mitochondrial mediated fashion and inhibited the migration of lung cancer cells and by metastasis.

1. Introduction

Lung cancer is the leading cause of cancer-related mortality worldwide, leading to an estimated 1.4 million death in 2010 [1]. Lung cancer is commonly classified into two major types, small cell lung carcinoma (SCLC) and non-small cell lung carcinoma (NSCLC). NSCLC constitutes 75% of lung cancer cases and is subdivided further into three major histological subtypes: adenocarcinoma (AC), squamous-cell carcinoma (SCC), and large-cell carcinoma. The AC and SCC subtypes represent 85% of NSCLC cases [2]. Emergence of resistance to anticancer drugs poses a major clinical challenge in successful treatment of cancer [3]. There is potential to overcome the two overriding problems in cancer chemotherapy the common occurrence of drug-resistant tumour cells and the lack of selectivity of cancer drugs in differentiating between cancerous cells and normal cells [4]. Following the discovery of the anti-tumour properties of cisplatin (*cis*-$Pt(NH_3)_2Cl_2$) and related complexes, attention for the discovery of new more efficient complexes of other metals and ligands developed. Against tumours the first to be entered for clinical trials were the analogues to cisplatin, complexes of palladium(II), *cis*-$Pd(en)Cl_2$ and *cis*-$Pd(DACH)_2Cl_2$ because palladium(II) has a very similar chemistry to platinum(II). Platinum

Abbreviations: CT-DNA, calf thymus DNA; EB, ethidium bromide; BSA, bovine serum albumin; A549, lung adenocarcinoma cell line; MTT, 3-(4,5-dimethylthiazol-2-yl)-2,5-diphenyltetrazolium bromide; LDH, lactate dehydrogenase; NO, nitric oxide; ROS, reactive oxygen species; DCFH-DA, 2′,7′ -dichlorofluoresceindiacetate; GSH, reduced glutathione; OPT, ortho-pthalaldehyde; SOD, superoxide dismutase; CAT, catalase; GST, glutathione-S-transferase; GPx, glutathione peroxidase; PI, propidium iodide; MPT, mitochondrial permeability transition; AIF, apoptosis-inducing factor; CAD, caspase-activated deoxyribonuclease.

* Corresponding authors.
E-mail addresses: rpnchemist@gmail.com, rpnchemist@rediffmail.com (R. Prabhakaran), k_natraj6@yahoo.com (K. Natarajan).

http://dx.doi.org/10.1016/j.ejmech.2014.05.075
0223-5234/

metallo-drugs are the most effective drugs used for the treatment of tumour though its clinical utility is restricted due to the frequent increase of drug resistance, the limited range of tumours against which these drugs are active and severe normal tissue toxicity being the nephrotoxicity an important side effect which interfere with their therapeutic efficiency [5–9]. These disadvantages have motivated the improvement of platinum-based anticancer drugs different from the traditional cisplatin structure and which could probably have different DNA-binding modes as well as show different biological profiles [10–14]. Several biological experiments have demonstrated that DNA is the major intracellular target of many anticancer drugs, cancerogens and viruses [15,16]. Interactions of small molecules at specific sites along a DNA strand as reactive models for protein–nucleic acid bindings, provide paths toward rational drug design as well as means to develop sensitive chemical probes for DNA [17,18]. Numerous metal complexes have been used as probes of DNA, as agents for mediation of strand scission of duplex DNA and as chemotherapeutic agents [19–26]. Thiosemicarbazones and their metal complexes have been expansively studied because they have a wide range of potential medical applications [27–30] which include notably antiparasital [31], antibacterial [32], antitumour activities [33], antiviral [34], fungicidal [35], and antineoplastic [36]. Such potential medical activities are owing to the strong chelating ability of thiosemicarbazones with biologically important metal ions such as Fe, Cu, Ni and their reductive capacities [37–41]. Nickel(II) complexes containing nitrogen and sulphur donor ligands are highly important [42–46] because several hydrogenases and carbon monoxide dehydrogenases [47] contain such nickel ion as their active site. In this line, analogues nickel complexes are found to be potent in various therapeutic applications [48–50]. With the expectation, platinum mimic nickel and palladium complexes also exhibiting significant cytotoxicity [51–54], we have already reported the biological evolution of 3-methoxy salicylaldehyde 4(*N*) substituted thiosemicarbazone complexes of palladium [53]. In this article, the new palladium complexes were exposed to study their effect on A549 and HepG2 cell lines. The MTT, LDH, NO and cellular uptake studies were done. However, in the present manuscript in addition to the above studies, we have done a detailed biological investigation of new nickel(II) complexes containing 3-methoxy salicylaldehyde 4(*N*) substituted thiosemicarbazone on lung carcinoma (A549) cells and mechanism of drug action leading to apoptosis has been explored.

2. Experimental section

2.1. Complex synthesis and characterization

The ligands $(H_2L)^{1-4}$ and the nickel precursor $[NiCl_2(PPh_3)_2]$ were synthesized according to the standard literature procedures [55,56]. All the reagents used were analar grade, were purified and dried according to the standard procedure [57]. The synthesis, analytical and spectral characterization of the ligands $(H_2L)^{1-4}$ were reported by our group earlier [53]. CT-DNA, EB and BSA were obtained from Sigma Aldrich, DMEM, FBS and all other cell-culture reagents were obtained from Hi-media Laboratories, India. Reagents for enzyme assays were obtained from Merck speciality Chemicals, India. Primary antibodies used were obtained from Cell signalling technology, USA and Upstate, USA. HRP-conjugated secondary antibodies, was purchased from Leinco Technologies, USA. Western-blot membranes were obtained from Whatman, USA. DCF was obtained from Calbiochem, USA. DiOC6 and CCCP were obtained from Sigma–Aldrich. Infrared spectra were measured as KBr pellets on a Nicolet Avatar Model FT-IR spectrophotometer in the 400–4000 cm^{-1} range. Elemental analysis of carbon, hydrogen, nitrogen, and sulphur were determined using Vario EL III CHNS at the Department of Chemistry, Bharathiar University, Coimbatore, India. The electronic spectra of the complexes have been recorded in dichloromethane using a JASCO V-630 Spectrophotometer in the 200–800 nm range. Emission spectra were recorded by using JASCO FP 6600 spectrofluorometer. ^1H NMR spectra were recorded in DMSO at room temperature with a Bruker 400 MHz instrument, chemical shift relative to tetramethylsilane. Melting points were measured in a Lab India apparatus. Single crystal data collections and corrections for the new Ni(II) complexes were done at 293 K with CCD kappa Diffractometer using graphite mono chromated MoKα (λ = 0.71073 Å) radiation [58–60]. The structural solutions were done by using SHELXTL-97 [61] and refined by full matrix least square on F^2 using SHELXL-97 [62].

2.1.1. Preparation of [Ni(Msal-tsc)(PPh$_3$)].Cl (**1**)

An ethanolic (25 ml) solution of $[NiCl_2(PPh_3)_2]$ (0.200 g; 0.3058 mmol) was slowly added to 3-methoxysalicylaldehydethiosemicarbazone [H_2-Msal-tsc] (0.068 g, 0.3058 mmol) in dichloromethane (25 ml). The mixture was allowed to stand for 4 days at room temperature. Reddish orange crystals formed were filtered, washed with petroleum ether (60–80 °C) and n-hexane. Yield: 58%. M.p. 288 °C. Anal. Calcd. for $C_{27}H_{25}ClN_3NiO_2PS$: C, 55.85; H, 4.34; N, 7.24; S, 5.52. Found: C, 55.02; H, 4.23; N, 7.05; S, 5.39%. FT-IR (cm^{-1}) in KBr: 1542 ($\nu_{C=N}$), 1318 (ν_{C-O}), 770 ($\nu_{C=S}$), 1441, 1100, 694 cm^{-1} (for PPh_3); UV–vis (CH_2Cl_2), λ_{max}: 257 (24,360) nm ($dm^3\ mol^{-1}\ cm^{-1}$) (intra-ligand transition); 341 (17,950), 364 (8290), 372 (8102) nm ($dm^3\ mol^{-1}\ cm^{-1}$) (LMCT s → d); ^1H NMR (DMSO-d6, ppm): 8.36 (s, 1H, CH=N), δ 9.12 (s, 1H, N(2)H–C=S–) 3.77 (s, 3H, OCH_3), 6.37–7.48 (m, aromatic) 7.90 and 8.08 (2s, 1H, NH_2).

The very similar method was followed to synthesize other complexes.

2.1.2. Preparation of [Ni(Msal-mtsc)(PPh$_3$)](**2**)

The complex **2** was prepared by the procedure as used for (**1**) with 3-methoxysalicylaldehyde-4(N)-methylthiosemicarbazone [H_2-Msal-mtsc] (0.074 g; 0.3058 mmol) and $[NiCl_2(PPh_3)_2]$ (0.200 g; 0.3058 mmol). Yield: 63%. M.p. 238 °C. Anal. Calcd. for $C_{28}H_{26}N_3NiO_2PS$: C, 60.24; H, 4.69; N, 7.52; S, 5.74. Found: C, 60.18; H, 4.63; N, 7.49; S, 5.68%. FT-IR (cm^{-1}) in KBr: 1556 ($\nu_{C=N}$), 1359 (ν_{C-O}), 738 (ν_{C-S}), 1450, 1068, 610 cm^{-1} (for PPh_3); UV–vis (CH_2Cl_2), λ_{max}: 257 (11,659), 303 (8265) nm ($dm^3\ mol^{-1}\ cm^{-1}$)(intra-ligand transition); 359 (7140) nm, 371 (7000) nm ($dm^3\ mol^{-1}\ cm^{-1}$) (LMCT s → d); 410 (6900) nm ($dm^3\ mol^{-1}\ cm^{-1}$) (forbidden (d → d) transition); ^1H NMR (DMSO-d6, ppm): 8.32 (s, 1H, CH=N), 8.30 (s, 1H, $NHCH_3$), 3.80 (s, 3H, OCH_3), 6.45–6.99 (m, aromatic), 1.13 (t, 3H, CH_3).

2.1.3. Preparation of [Ni(Msal-etsc)(PPh$_3$)] (**3**)

The complex **3** was prepared by the procedure as used for (**1**) with 3-methoxysalicylaldehyde-4(N)-ethylthiosemicarbazone [H_2-Msal-etsc] (0.078 g; 0.3058 mmol) and $[NiCl_2(PPh_3)_2]$ (0.200 g; 0.3058 mmol). Yield: 64%. M.p. 244 °C. Anal. Calcd for $C_{29}H_{28}N_3O_2SNiP$: C, 60.86; H, 4.93; N, 7.34; S, 5.60. Found: C, 60.81; H, 4.87; N, 7.29; S, 5.52%. FT-IR (cm^{-1}) in KBr: 3310 (ν_{OH}), 1536($\nu_{C=N}$), 1276 (ν_{C-O}), 795 (ν_{C-S}), 1452, 1089, 697 cm^{-1} (for PPh_3); UV–vis (CH_2Cl_2), λ_{max}: 232 (21,150) nm ($dm^3\ mol^{-1}\ cm^{-1}$) (intra-ligand transition), 362 (18,560) nm, 371 (17,450) nm ($dm^3\ mol^{-1}\ cm^{-1}$) (LMCT s → d); ^1H NMR (DMSO-d6, ppm): 8.54 (s, 1H, CH=N), 7.78 (br s, 1H, NHC_2H_5), 3.75 (s, 3H, OCH_3), 6.79–7.78 (m, aromatic), 3.13–3.14 (m, 2H, CH_2), 1.04 (t, 3H, CH_3).

*2.1.4. Preparation of [Ni(Msal-ptsc)(PPh$_3$)] (**4**)*

The complex **4** was prepared by the procedure as has been used for (**1**) with 3-methoxysalicylaldehyde-4(N)-phenylthiosemicarbazone [H_2-Msal-ptsc] (0.092 g; 0.3058 mmol) and [$NiCl_2(PPh_3)_2$] (0.200 g; 0.3058 mmol).Yield: 74%. M.p. 261 °C. Anal. Calcd. for $C_{33}H_{28}N_3O_2S$-NiP: C, 63.89; H, 4.55; N, 6.77; S, 5.17. Found: C, 63.82; H, 4.49; N, 6.73; S, 5.11%. FT-IR (cm^{-1}) in KBr: 1554 ($\nu_{C=N}$), 1310 (ν_{C-O}), 743 (ν_{C-S}), 1435, 1096, 694 cm^{-1} (for PPh_3); UV–vis (CH_2Cl_2), λ_{max}: 238 (15,270) nm (dm^3 mol^{-1} cm^{-1}) (intra-ligand transition); 366 (14,360), 375 (13,650) nm (dm^3 mol^{-1} cm^{-1}) (LMCT s → d), 424 (12,800) nm (dm^3 mol^{-1} cm^{-1}) (forbidden (d → d) transition); ^{1}H NMR (DMSO-d6, ppm): 8.70 (s, 1H, CH═N), 9.44 (s, 1H, NHPh), 3.41 (s, 3H, OCH_3), 6.61–7.87 (m, aromatic).

2.2. DNA binding study

Various concentrations (0.05–0.5 μM) of CT-DNA solution was dissolved in a tris HCl buffer (pH 7) were added to the nickel complexes **1**–**4** (1 μM). Absorption spectra were recorded after equilibrium at 20 °C for 10 min. Emission measurements were carried out by using a JASCO FP- 6600 spectrofluorimeter. Tris–buffer was used as a blank to make preliminary adjustments. The excitation wavelength was fixed and the emission range was adjusted before measurements. All measurements were made at 20 °C. For emission spectral titrations, complex concentration was maintained constant as 1 μM and the concentration of DNA was varied from 0.05 to 0.5 μM. The emission enhancement factors were measured by comparing the intensities at the emission spectral maxima under similar conditions. In order to find out the mode of attachment of CT DNA to the complexes (**1**–**4**) fluorescence quenching experiments of EB-DNA were carried out by adding 10 μM nickel(II) complexes with 10 μl every time to the samples containing 12 μM EB, 12 μM DNA and tris-buffer (pH = 7). Before measurements, the system was shook and incubated at room temperature for ~5 min. The emission was recorded at 530–750 nm.

2.3. Bovine serum albumin binding study

The protein binding study was performed by tryptophan fluorescence quenching experiments using bovine serum albumin (BSA, 1 μM) as the substrate in phosphate buffer (pH 7). Quenching of the emission intensity of tryptophan residues of BSA at 347 nm (excitation wavelength at 278 nm) was monitored using complexes **1**–**4** as quenchers with increasing complex concentration. Synchronous fluorescence spectra of BSA with various concentrations of complexes were obtained from 300 to 400 nm when $\Delta\lambda$ = 60 nm and from 290 to 500 nm when $\Delta\lambda$ = 15 nm. The excitation and emission slit widths were 5 and 6 nm, respectively. Fluorescence and synchronous measurements were performed using a 1 cm quartz cell on a JASCO FP 6500 spectrofluorimeter.

2.4. Cell-culture

Human lung adenocarcinoma cells, A549 were obtained from NCCS, Pune, India. Cells were grown in DMEM and 10% FBS (v/v), containing 100 units/ml penicillin, 30 μg/ml streptomycin and 20 μg/ml gentamicin in a CO_2 incubator with 5% CO_2.

2.4.1. Cell proliferation (MTT) assay

Effect of the complexes on the viability of human lung cancer cells (A549) was assayed by the 3-(4,5-dimethylthiazol-2-yl)-2,5-diphenyltetrazolium bromide (MTT) assay [63]. The cells were seeded at a density of 10,000 cells per well, in 200 μl DMEM medium and were allowed to attach overnight in a CO_2 incubator. Then flick off the media and the complexes (**1**–**4**) dissolved in DMSO and diluted in cell culture media were added to the cells at a final concentration of 1, 10, 25 and 50 μM. After 48 h, the wells were treated with 20 μl MTT (5 mg/ml PBS) and incubated at 37 °C for 4 h. The purple formazon crystals formed were dissolved in 200 μl DMSO and read at 570 nm in a micro plate reader.

2.4.2. Release of lactate dehydrogenase (LDH)

LDH activity was determined by the linear region of a pyruvate standard graph using regression analysis and expressed as percentage (%) leakage as described previously [64]. Briefly, to a set of tubes, 1 ml of buffered substrate (lithium lactate) and 0.1 ml of the media or cell extract were added and tubes were incubated at 37 °C for 30 min. After adding 0.2 ml of NAD solution, the incubation was continued for another 30 min. The reaction was then arrested by adding 0.1 ml of DNPH reagent and the tubes were incubated for further period of 15 min at 37 °C. After this, 0.1 ml of media or cell extract was added to blank tubes after arresting the reaction with DNPH. 3.5 ml of 0.4 N sodium hydroxide was added to all the tubes. The colour developed was measured at 420 nm in a Shimadzu UV/visible spectrophotometer. The amount of LDH released was expressed as percentage.

2.4.3. Nitric oxide (NO) assay

The amount of nitrite was determined by the method of Stuehr and Marletta [65]. Nitrite reacts with Griess Reagent to give a coloured complex measured at 540 nm. To 100 μl of the medium, 50 μl of Griess reagent I was added, mixed and allowed to react for 10 min. This was followed by 50 μl addition of Griess reagent II, the reaction mixture was mixed well and incubated for another 10 min at room temperature. The intensity of pink colour developed was measured at 540 nm in a microquant plate reader (Biotek Instruments).

2.4.4. Wound healing assay

For cell motility determination, A549 cells (1×10^5 cells/ml) were plated in six well tissue culture plates and grown to 80–90% confluence. After aspirating the medium, the centres of the cell mono layers were scraped with a sterile micropipette tip to create a denuded zone (gap) of constant width. Subsequently, cellular debris was washed with PBS, and A549 cells were exposed to complexes **1**–**4**. The wound closure was monitored and photographed at 48 h with an Olympus inverted microscope and camera.

2.4.5. Reactive oxygen species (ROS) generation

Relative changes in intracellular reactive oxygen species in A549 cells were monitored using a fluorescent probe, 2′,7′-dichlorofluoresceindiacetate (DCFH-DA) [66].The treatment groups were maintained as described for LDH leakage and a time course for ROS generation by complexes was done. Cells were incubated with 10 μM of DCFH-DA and incubated for 30 min, followed by incubation with complexes (**1**–**4**) for different time periods (15 min, 30 min and 1 h). One treatment group with 50 μM H_2O_2 was included to serve as a positive control. Cells were then harvested, centrifuged, washed and re suspended in PBS and read in a Hitachi spectrofluorimeter using excitation 480 nm, emission 520 nm. The estimations were carried out thrice in triplicate, ensuring each time that the number of cells per treatment group were the same to ensure reproducibility. The values were expressed as % relative fluorescence as compared to the control.

2.4.6. Cellular antioxidant status

After completing the treatment schedule, cell extracts were prepared by sonication in Tris-EDTA-PMSF buffer and the protein

content of the supernatant was determined by Lowry method [67] and used for antioxidant assays. Both reagent blanks and enzyme blanks were measured for all assays. All assays were carried out in the linear range and expressed as specific activities of enzymes. The intracellular concentration of reduced glutathione was estimated by the fluorometric assay as described by Pereira-Caro et al. [68] using ortho-phthalaldehyde (OPT). Superoxide dismutase (SOD) [69], Catalase (CAT) [70], Glutathione-S-transferase (GST) [71], and Glutathione peroxidase (GPx) [72] activities were determined as described previously.

2.4.7. Measurement of mitochondrial transmembrane potential

Mitochondrial energization was determined as the retention of the dye 3, 3′ dihexyloxacarbocyanine iodide [$DiOC_6$ (3)] in normal cells and exclusion by the cells with mitochondrial membrane damage. Cells were treated with complexes **1**–**4** as described in LDH leakage experiment. After the treatment period the medium was flicked off and washed twice with PBS. Then the cells were treated with 50 nM [$DiOC_6$ (3)] at 37 °C for 30 min and the cells were washed twice with PBS. The cells were collected, re-suspended in 2 ml PBS and fluorescence intensity was measured in a fluorescent spectrophotometer using Excitation/Emission as 488 nm/500 nm.

2.4.8. Apoptotic cell detection by propidium iodide

After treatment with complexes for 48 h, the cells were collected, washed with PBS, fixed overnight with 70% ethanol at 4 °C, and incubated with propidium iodide at room temperature for 30 min. Nuclear morphology was examined using fluorescence microscope.

2.4.9. Western blot analysis

Cells were collected and washed twice in PBS, then lysed in ice-cold lysis buffer (50 mM Tris–HCl, pH-7.4, 150 mM NaCl, 5 mM EDTA, 50 mM NaF, 1% Triton X-100, 1 mM sodium-orthovanadate, 1 mM phenylmethanesulfonylfluoride, 1 mg/ml aprotinin, 2 μg/ml pepstatin-A, and 2 μg/ml leupeptin) on ice for 1 h. Cell lysates were then centrifuged for 15 min at 13,000 rpm at 4 °C. Proteins were separated using SDS-PAGE and transferred to PVDF membrane. The blots were blocked with 5% non-fat milk in TBST at RT for 1 h and incubated overnight with the appropriate primary antibody at 4 °C. After wash, the blots were incubated with peroxidase-conjugated secondary antibody for 1 h. Bands were monitored using DAB system. GAPDH were used as an internal control.

2.5. DNA fragmentation

DNA fragmentation analysis was carried by the method of Gong et al. [73]. The cells are prefixed in 70% ethanol, DNA is extracted with 0.2 M phosphate-citrate buffer at pH-7.8, and the extract is sequentially treated with RNase A and proteinase K and then subjected to electrophoresis.

3. Results and discussion

The stoichiometric reactions of $[NiCl_2(PPh_3)_2]$ with a series of 3-methoxysalicylaldehyde-4(*N*)-substituted thiosemicarbazones $(H2L)^{1-4}$ in 1:1 ethanol/dichloromethane resulted in the formation of new complexes **1**–**4** (Scheme 1), where the substituted thiosemicarbazones acted as a tridentate ONS ligand. Among them, $H2L^1$ acted as a monobasic tridentate and $(H2L)^{2-4}$ acted as dibasic tridentate ligands. The analytical data of which confirmed the stoichiometry of the complexes (**1**–**4**). The structures of the complexes (**1**, **2** and **4**) were confirmed by the X-ray crystallographic study. The new complexes (**1**–**4**) are soluble in common organic solvents such as dichloromethane, chloroform, benzene, acetonitrile, ethanol, methanol, dimethylformamide and dimethylsulfoxide.

3.1. Spectroscopic studies

The infrared spectra of the ligands $(H2L)^{1-4}$ exhibited ν(OH) vibration in the region 3339–3458 cm^{-1}, which disappeared completely after complexation with the nickel(II) ion showing deprotonation prior to coordination through oxygen atom in all the four complexes (**1**–**4**). It is further confirmed with the downfield shift of 28–43 cm^{-1} for $\nu_{(C-O)}$ [74]. An azomethine nitrogen $\nu_{(C=N)}$ band appeared at the region 1536–1593 cm^{-1} in the ligands has been shifted to lower frequency in all the complexes (1536–1556 cm^{-1}) indicating the coordination of azomethine nitrogen atoms [75]. As the ligand contains a thioamide (–NH–C=S) functional group it may exist in thione-thiol tautomerization. The absence of the $\nu_{(S-H)}$ stretch in the region 2500–2600 cm^{-1} and presence of $\nu_{(N-H)}$ stretch in the region 3150–3350 cm^{-1} in the IR spectrum of the ligands indicate thione form in the solid state. This is further confirmed from the presence of a strong band in the region 771–795 cm^{-1} corresponding to the $\nu_{(C=S)}$ stretching which was completely disappeared in the spectra of the new complexes **2**–**4** and the appearance of a new band at 738–743 cm^{-1} due to $\nu_{(C-S)}$ vibration, indicated the coordination of the sulphur atom after enolisation followed by deprotonation [76,77]. However, the absence of the $\nu_{(S-H)}$ stretch and presence of $\nu_{(N-H)}$ stretch at 3055 cm^{-1} for complex **1** indicate the involvement of the thione sulphur in the coordination rather than thiolate [51]. Moreover, the characteristic absorption bands corresponding to the presence of triphenylphosphine were also present in the expected region [75]. The electronic spectra of nickel(II) complexes displayed four to five bands in the region around 232–424 nm. The band appeared at 232–303 nm has been assigned to intra ligand transition and the band at 341–375 nm to LMCT (s → d) and the shoulder at 410–424 nm to forbidden (d → d) transition [78,79]. The ^1H NMR spectra of the ligands $(H2L)^{1-4}$ and the corresponding complexes (**1**–**4**) recorded in DMSO showed all the expected signals. In the spectra of $(H2L)^{1-4}$, a sharp singlet corresponding to the phenolic –OH group has appeared at 11.34–11.76 ppm (Fig. S1–S8). However, this singlet completely disappeared in all the four complexes confirmed the involvement of phenolic oxygen in coordination

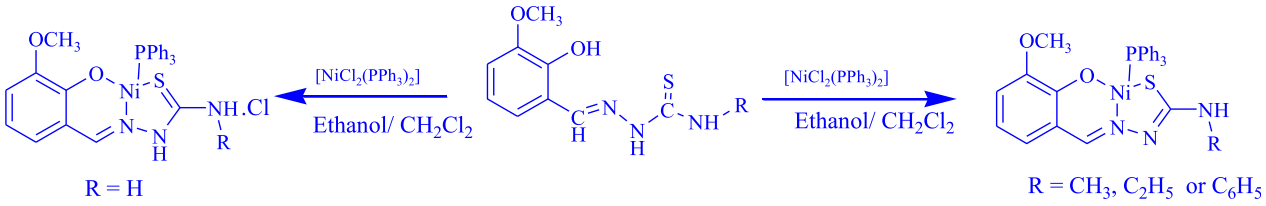

Scheme 1. Preparation of new nickel (II) complexes.

[54]. The spectra of (H2L) **1**–**4**showed a singlet at δ 9.13–10.0 ppm corresponding to (N(2)H–C═S) group [80], but in complexes **2**–**4** there was no resonance attributable to N(2)H, indicating coordination of the thiolate sulphur atom of the ligand in the anionic form after deprotonation at N(2). However, in the spectrum of complex **1**, a singlet occurred at δ 9.12 ppm corresponding to (N(2)H–C═S–) group indicating the thionic form of ligand even after complexation [51]. In the spectra of $H2L^{1-4}$ and the complexes, a complex multiplet appeared at 6.37–7.87 ppm was assigned to aromatic protons of the ligands and triphenylphosphine [75] and a singlet corresponding to the $-OCH_3$ group occurred at the 3.41–3.80 ppm range [53]. Two singlets observed at 8.37–8.40 ppm and 8.37–9.40 ppm have been assigned to azomethine and terminal –NH protons of the ligands **2**–**4**. Whereas, in the complexes a singlet at 8.30–8.70 ppm was observed for the presence of azomethine protons and another singlet observed around 8.12–9.20 ppm in the complexes **2**, **3** and **4** was assigned to the terminal NH protons of the ligands. Moreover, in complex **1**, there were two broad singlets appeared at 7.90 and 8.08 ppm corresponding to NH_2 protons of the coordinated ligand. A triplet observed around 1.03–2.90 ppm in the spectra of $H2L^2$, $H2L^3$ and the complexes (**2** and **3**), was assigned to the presence of methyl group of protons. Further, a multiplet at 3.12–3.58 ppm was also observed corresponding to the methylene protons of $H2L^3$ and complex **3** [53].

3.2. X-ray crystallography

The ORTEP diagram of the complexes **1**, **2** and **4** with the numbering scheme is shown in Figs. 1–3 and S9. The most significant parameters for these compounds are shown in Tables 1 and 2. Crystallographic analysis revealed that complexes **1**, **2** and **4** crystallized in the monoclinic crystal system with space group, C2/c, Cc and P21 respectively. Among the ligands $(H2L)^{1,2,4}$, $H2L^1$ acted as a monobasic tridentate whereas, $(H2L)^2$ and $(H2L)^4$ acted as a dibasic tridentate. In the complex **1**, the ligand $(H2L)^1$ coordinated to nickel by utilizing its phenolic oxygen, N1 nitrogen and thione sulphur atoms by forming one six member and another five member ring with a bite angle of [88.0(1) (S–Ni–N(1))]. The presence of a chloride ion outside the coordination sphere compensates the charge of nickel as Ni^{2+}, giving ionic nature to the complex (**1**). The Ni–S 2.144(1) Å, Ni–P 2.2130 Å, Ni–N 1.892(3) Å and Ni–O

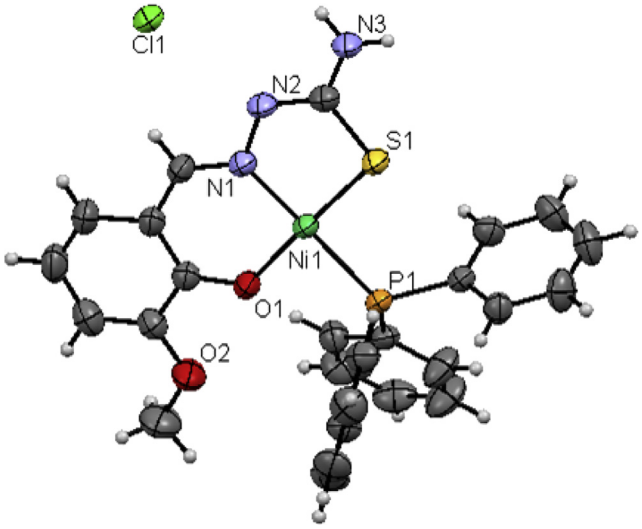

Fig. 1. ORTEP diagram of [Ni(Msal-tsc)(PPh_3)].Cl (**1**), (Solvent moiety is removed for clarity and Thermal ellipsoids are shown at 50% probability).

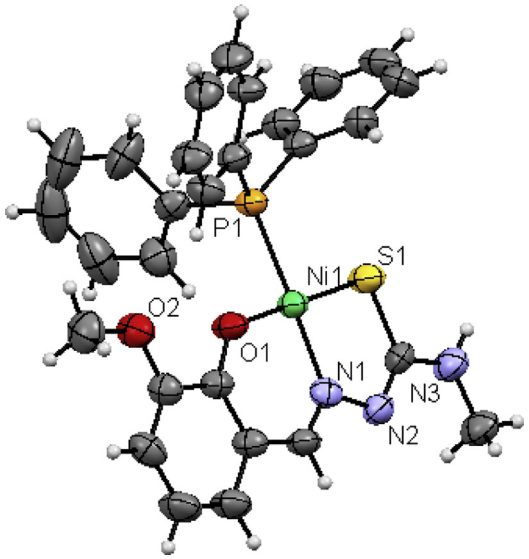

Fig. 2. ORTEP diagram of [Ni(MSal-mtsc)(PPh_3)](**2**) (Thermal ellipsoids are shown at 50% probability).

1.850(3) Å bond lengths are comparable with the values of already reported ionic complex [51]. From the ^1H NMR spectral studies, there was a detectable proton signal at δ 9.12 ppm corresponding to the (N(2)H–C═S) group. However, the position of this proton (hydrogen) could not be located in the X-ray crystallographic analysis. While dealing with the hydrogen bonding, we could be able to find the (D … A) distance corresponding to the N(2) … Cl(1) bond between the imine nitrogen and the chloride ion which was present outside the coordination sphere. The chloride ion involved in one intra molecular hydrogen bonding with imine nitrogen and inter molecular hydrogen bonding with (H3A) and (H3B) protons of N(3) amine of second and third molecules respectively (Table S1). Interestingly, this intra and inter molecular hydrogen bonding resulting a 2D network which contains parallelogram like structure generated by two chloride ions and two amine nitrogen atoms (Fig. S9). The variation in the Ni–N, Ni–O, Ni–S and Ni–P bond distances and significant deviation from ideal angle S(1)-Ni-O(1) [177.52(9)°] and P(1)–Ni–N(1) [176.8(1)°] brought a distorted square planar geometry to the molecule.

In the complexes **2** and **4**, the Ni(II) ion is coordinated to the dibasic tridentate ligands through thiolate sulphur (Ni–S bond

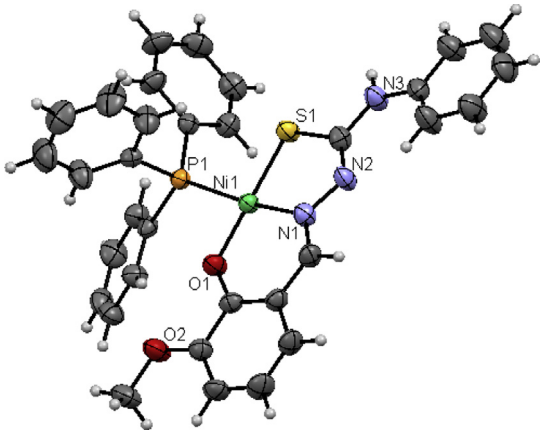

Fig. 3. ORTEP diagram of [Ni(Msal-ptsc)(PPh_3)](**4**) (Thermal ellipsoids are shown at 50% probability).

Table 1
Crystallographic data of new Ni(II) thiosemicarbazone complexes.

	[Ni(Msal-tsc)(PPh_3)].Cl (**1**)	[Ni(MSal-mtsc)(PPh_3)] (**2**)	[Ni(Msal-ptsc)(PPh_3)] (**4**)
Empirical Formula	$C_{27}H_{25}$ $ClN_3NiO_{2.5}PS$	$C_{28}H_{26}N_3NiO_2PS$	$C_{33}H_{28}N_3O_2PNiS$
Formula Weight	588.69	558.26	620.32
Crystal System	Monoclinic	Monoclinic	Monoclinic
Space Group	C2/c	Cc	$P2_1$
Wavelength	0.71073 Å	0.71073 Å	0.71073 Å
Temperature	293(2)	293(2)	293(2)
a	22.4947(6) Å	18.460(1) Å	11.7861(3) Å
b	18.1347(5) Å	10.6291(7) Å	8.0188(2) Å
c	14.5681(4) Å	13.610(1) Å	15.6057(5) Å
α	90°	90°	90°
β	106.329(1)°	96.013(4)°	101.696(1)°
γ	90°	90°	90°
V	5703.1(3) $Å^3$	2655.8(3) $Å^3$	1444.28(7) $Å^3$
Crystal size	0.08 × 0.18 × 0.18 mm	0.06 × 0.08 × 0.20 mm	0.08 × 0.16 × 0.22 mm
Z value	8	4	2
Limiting indices	$-18 \le h \le 30$, $-24 \le k \le 19$, $-18 \le l \le 18$	$0 \le h \le 25$, $0 \le k \le 14$, $-18 \le l \le 17$	$0 \le h \le 16$, $0 \le k \le 10$, $-21 \le l \le 20$
D_{calc}	1.371	1.396	1.426
Reflections collected/unique	32619/7221 [R(int) 0.102]	15187/3374 [R(int) 0.111]	13636/3956 [R(int) 0.072]
Theta range for data collection	2.25–29.01°	3.55–28.98°	2.42–29.01°
F_{000}	2432	1160	644
Goodness-of-fit on F^2	1.017	1.109	1.04
Refinement method	Full-matrix least-squares on F^2	Full-matrix least-squares on F^2	Full-matrix least-squares on F^2
μ (MoKα)	0.934	0.900	0.835
Completeness to theta $2\theta_{max}$	29.01°	28.98°	29.01°
Data/restraints/parameters	7221/0/349	3374/2/326	3956/1/371
Final R indices [$I > 2$sigma(I)]	R1 = 0.0562, wR2 = 0.1298	R1 = 0.0552, wR2 = 0.1234	R1 = 0.0463, wR2 = 0.0979
R indices (all data)	R1 = 0.1414, wR2 = 0.1637	R = 0.1134, wR2 = 0.1524	R1 = 0.0695, wR2 = 0.1099
Largest diff. peak and hole	0.496 and −0.572 e A^{-3}	0.408 and −0.877 e A^{-3}	0.983 and −0.444 e A^{-3}

distances of 2.131(2) A° and 2.158(1) A° respectively), phenolic oxygen (Ni–O bond distances of 1.855(5) A° and 1.845(3) A° respectively) and the nitrogen atom (Ni–N bond distances of 1.911(7) A° and 1.889(4) A° respectively). The remaining binding site is occupied by the triphenylphosphine unit (Ni–P(1) bond distances of 2.224(2) A° and 2.226(1) A° respectively) with a bite angle [S(1)–Ni(1)–N(1)] of 86.4(2)° for **2** and 85.8(1)° for **4**. The Ni–S, Ni–P, Ni–O and Ni–N bond lengths are comparable with those of the reported complexes [51,52,74,81]. The [S(1)–Ni(1)–O(1)] bond angles found are 178.5(2)° for **2** and 178.6(1)° for **4** and [P(1)–Ni(1)–N(1)] bond angles found are 173.3(2)° for **2** and 171.6(1)° for **4** which deviate considerably from the ideal angle of 180° causing significant distortion in the square planar geometry of the complexes. It is observed from the *trans* angle [P(1)–Ni(1)–N(1)] of the above said complexes, the deviation from the ideal geometry is a bit more in **4** as compared with **1** and **2**.

3.3. DNA binding studies

For evaluating the anticancer property of any newly synthesized complex, DNA binding is the predominant property looked for in pharmacology and hence, the interaction between DNA and metal complexes is of paramount importance in understanding the mechanism. Thus, the mode and propensity for binding of the new nickel(II) complexes **1**–**4** to CT DNA were studied with the help of electronic absorption and fluorescence quenching techniques.

The absorption spectra of complexes (**1**–**4**) at constant concentration (1 μM) and with different concentrations of CT-DNA (0.05–0.50 μM) are given in Fig. 4. The absorption spectra of complex **1** mainly consist of four resolved bands [intra ligand (IL) and charge transfer (CT) transitions] centred at 257 nm (IL), 341 nm, 364 nm and 372 nm (CT). As the DNA concentration is increased, the hypochromism of 85.45% with a blue shift of 3 nm was observed in the intra ligand band. The CT bands at 341, 364 and 372 nm showed modest hyperchromism with negligible absorption shifts. In addition, the binding of complex **1** to CT DNA led to isosbestic spectral change with the isosbestic point at 302 nm. For complex **2**, upon addition of DNA, the intra ligand band at 257 nm exhibited hypochromism of 92.79% with a 9 nm blue shift. The CT band at 359 nm showed 22.35% of hyperchromism without the wavelength shift in the absorption maxima. The binding behaviour of complexes **3** and **4** is quite similar. As the DNA concentration is increased, the intra ligand band at 258 nm (for **3**) and 257 nm (for **4**) exhibited hypochromism of 93.01% and 73.84% respectively with 2–5 nm blue shift. The CT bands showed slight hyperchromism at 362, 371 nm (for **3**) and 375, 424 nm (for **4**) without any shift upon

Table 2
Selected bond lengths (Å) and angels (°) for Ni(II) thiosemicarbazone complexes.

Atoms	[Ni(Msal-tsc)(PPh_3)].Cl (**1**)	[Ni(Msal-mtsc)(PPh_3)] (**2**)	[Ni(MSal-ptsc)(PPh_3)] (**4**)
Ni–S(1)	2.144(1)	2.131(2)	2.158(1)
Ni–P(1)	2.2130	2.224(2)	2.226(1)
Ni–O(1)	1.850(3)	1.855(5)	1.845(3)
Ni–N(1)	1.892(3)	1.911(7)	1.889(4)
S(1)–Ni–P(1)	91.65(4)	90.35(9)	89.86(5)
S(1)–Ni–O(1)	177.52(9)	178.5(2)	178.6(1)
S(1)–Ni–N(1)	88.0(1)	86.4(2)	85.8(1)
P(1)–Ni–O(1)	86.51(9)	89.7(2)	89.3(1)
P(1)–Ni–N(1)	176.8(1)	173.3(2)	171.6(1)
O(1)–Ni–N(1)	93.8(1)	93.7(3)	95.2(2)

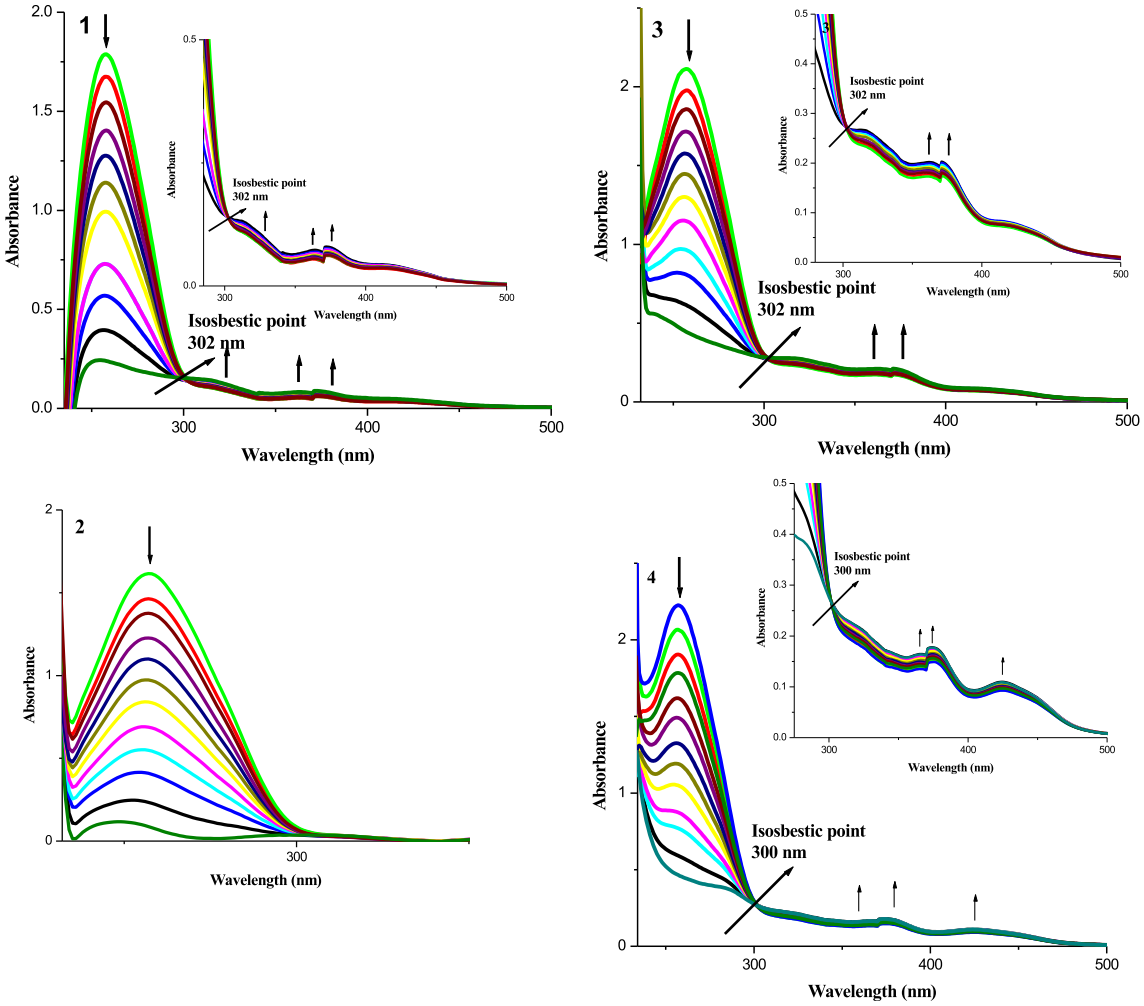

Fig. 4. Absorption titration spectra of **1**–**4** with increasing concentrations (0.05–0.5 μM) of CT-DNA (tris HCl buffer, pH 7).

addition of CT-DNA. A distinct isosbestic point appeared at 302 nm and 300 nm for complexes **3** and **4**. The observed hypochromic effect with blue shift suggested that complexes (**1**–**4**) bind to CT-DNA by intercalation mode [82]. The intrinsic binding constant K_b was determined by using Stern–volmer equation (1) [83,84].

$$[DNA]/[\varepsilon_a - \varepsilon_f] = [DNA]/[\varepsilon_b - \varepsilon_f] + 1/K_b[\varepsilon_b - \varepsilon_f] \quad (1)$$

The absorption coefficients ε_a, ε_f, and ε_b correspond to A_{obsd}/[complex], the extinction coefficient for the free complex and the extinction coefficient for the complex in the fully bound form, respectively. The slope and the intercept of the linear fit of the plot of [DNA]/[ε_a–ε_f] versus [DNA] give 1/[ε_a–ε_f] and 1/K_b[ε_b–ε_f], respectively. The magnitude of the binding strength of compounds with CT DNA was calculated by the intrinsic binding constant K_b (Table 3), which can be determined by monitoring the changes in the absorbance in the IL band at the corresponding λ_{max} with increasing concentration of DNA and is given by the ratio of the slope to the *Y* intercept in plots of [DNA]/(ε_a–ε_f) versus [DNA] (Fig. 5). From the binding constant values, it is inferred that complex **3** exhibited better binding than other complexes.

Table 3
Binding constant for interaction of complexes with CT-DNA.

System	K_b ($\times 10^5$ M^{-1})
CT-DNA + 1	0.502
CT-DNA + 2	1.445
CT-DNA + 3	1.697
CT-DNA + 4	0.230

The emission spectra of new nickel (II) complexes **1**–**4** showed fluorescence emission at 412, 715, 509 and 409 nm respectively (Fig. S10). Addition of CT DNA to the complex solution resulted in hypochromism of 37.46%, 63.97%, 81.26% and 16.69% respectively for complexes **1**–**4** by decreasing intensity with 1–2 nm blue shifts in the absorption maxima. The marked decreases in the fluorescence intensity of complexes indicate the intercalative binding mode of DNA. The binding of the complexes **1**–**4** to CT-DNA through intercalation mode has further been confirmed by competitive fluorescence quenching experiments. EB (3,8-diamino-5-ethyl-6-phenylphenanthrium bromide) is an intercalator that gives a significant increase in fluorescence emission when bound to DNA and it can be quenched by the addition of second DNA binding molecule by either replacing the EB and/or by accepting the excited state electron of the EB through a photo-electron transfer mechanism. Upon addition of complexes **1**–**4** to CT-DNA which was pretreated with EB caused significant reduction in the emission intensity at 605 nm (Fig. S11). Which indicates that the replacement of the EB fluorophore by respective complexes. The quenching extents of **1**–**4** were evaluated qualitatively by employing Stern–Volmer equation (2).

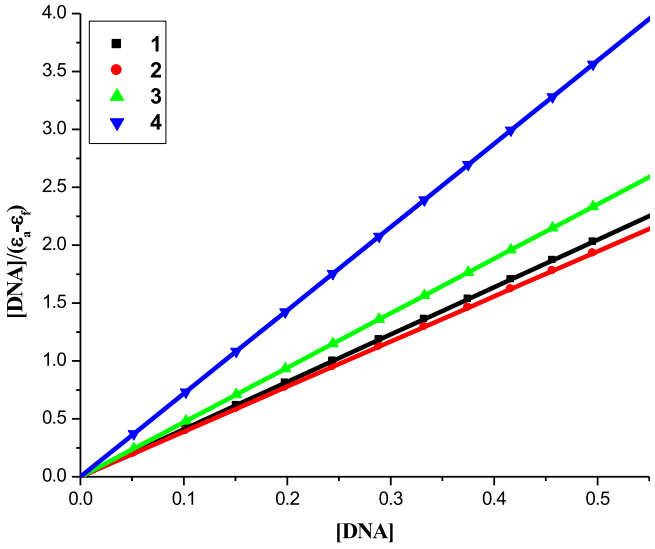

Fig. 5. Binding isotherms of the complexes **1**–**4** with CT-DNA.

$$I_0/I = K_{sv}[Q] + 1 \quad (2)$$

where I_0 is the emission intensity in the absence of compound, I is the emission intensity in the presence of compound, K_{sv} is the quenching constant, and [Q] is the concentration of the compound. The K_{sv} values have been obtained as a slope from the plot of I_0/I versus [Q] (Fig. S12). It was found to be 4.33×10^3, 5.19×10^3, 5.31×10^3 M^{-1} and 3.87×10^3 M^{-1} respectively for complexes **1**–**4**, Further, the apparent DNA binding constants (Kapp) were calculated using eqn (3):

$$K_{EB}[EB] = K_{app}[complex] \quad (3)$$

where [complex] is the value at 50% reduction in the fluorescence intensity of EB, K_{EB} (1.0×10^7 M^{-1}) is the DNA binding constant of EB, [EB] is the concentration of EB = 12 μM). K_{app} values were 5.19×10^5, 6.22×10^5, 6.37×10^5 and 4.64×10^5 M^{-1} for complexes **1**–**4** respectively. From these experimental data, it is seen that the complex **3** replaces the EB more effectively than the other complexes, which is in agreement with the results observed from DNA binding study. Furthermore, the observed quenching constants and binding constants of the new complexes suggest that the interaction of all the complexes with DNA may be intercalative.

3.4. Quenching mechanism of BSA by complexes

Bovine serum albumin (BSA) is the most extensively studied serum albumin, due to its structural homology with human serum albumin (HSA). Binding of Schiff base metal complexes with the most abundant carrier proteins (serum albumins) have also been an area of interest as such drug–protein binding greatly influences absorption, drug transport, storage, metabolism and excretion properties of typical drugs in vertebrates [85]. In addition, it has been shown that binding of Schiff-base metal complexes to bovine serum albumin (BSA) have enhanced the antioxidant capacity of BSA in ROSs scavenging for about more than 10-times [86]. Since serum albumins are well known to bind with small aromatics, the possible binding interactions of the nickel(II) thiosemicarbzone complexes (**1**–**4**) with BSA have been investigated by absorption/emission-titration experiments at room temperature. In the absorption spectra of BSA, the addition of 10 μM concentrations of the four complexes (**1**–**4**) (Fig. S13) showed enhanced absorption intensity of BSA with a blue shift of complex–BSA spectrum (from 273 to 269 nm). The formation of non-fluorescence ground-state complex induced the change in absorption spectrum of fluorophore and possible quenching mechanism of BSA by complexes (**1**–**4**) was found as static quenching [87].

3.4.1. Fluorescence quenching studies of BSA

A solution of BSA (1 μM) was titrated with various concentrations of the complexes (0–25 μM). Fluorescence spectra were recorded in the range of 290–500 nm upon excitation at 280 nm. The changes observed on the emission spectra of BSA by the addition of increasing amounts of the complexes (**1**–**4**) which are shown in Fig. 6. Upon the addition of complexes **1**–**4** to BSA, a significant decrease in the fluorescence intensity was observed at 347 nm with hypochromism of 87.74%, 93.36%, 93.67% and 86.12% respectively accompanied by 1–6 nm blue shifts. The observed quenching may be attributed to the possible changes in secondary structure of protein and this indicating the binding of complex to BSA [88]. According to Stern–Volmer quenching equation, eq (2). The K_{SV} value was found to be 6.37×10^5 M^{-1}, 6.49×10^5 M^{-1}, 1.33×10^6 M^{-1} and 2.94×10^5 M^{-1} corresponding to complexes **1**, **2**, **3** and **4** respectively. The observed linearity in the plots (Fig. S14; Table 4) indicates the ability of the complexes to quench the emission intensity of BSA. From K_{SV} values, the complex **3** exhibited better protein-binding ability with enhanced hydrophobicity. The results obtained from protein binding are reliable with its strong DNA binding affinity. For the static quenching interaction, if it is assumed that there are similar and independent binding sites in the biomolecule, the binding constant (K_b) and the number of binding sites (n) can be determined according to the method [89] using the Scatchard equation (4).

$$\log[(I_0 - I)/I] = \log K_b + n \log[Q] \quad (4)$$

where, in the present case, K_b is the binding constant for the complex–protein interaction and 'n' is the number of binding sites per albumin molecule, which can be determined by the slope and the intercept of the double logarithm regression curve of log [(I_0–I)/I] versus log[Q] (Fig. S15; Table 4).

3.4.2. Synchronous fluorescence spectroscopic studies of BSA

Synchronous fluorescence spectral study involves simultaneous scanning of the excitation and emission monochromators while maintaining a constant wavelength interval between them. It was used to obtain information about the molecular environment in the vicinity of the fluorophore moieties of BSA [90]. Synchronous fluorescence spectra show tyrosine residues of BSA only at the wavelength interval $\Delta\lambda$ of 15 nm whereas tryptophan residues of BSA at $\Delta\lambda$ of 60 nm. The amount of complexes (**1**–**4**) added to BSA (1 μM) is increased; there is a decrease in the intensity of the fluorescence spectral band corresponding to tyrosine residue with a red shift (1–5 nm) (Fig. S16). In addition, significant decrease of fluorescence intensity of tryptophan residues together with a small red shift (1–2 nm) in the emission wavelength was also observed for the complexes except **4** which displayed hypochromism (Fig. S17). These experimental results indicate that the metal complexes do affect the microenvironment of both tyrosine and tryptophan residues during the binding process and synchronous measurements confirmed the effective binding of all the complexes with BSA.

3.5. Effect of Ni(II) thiosemicarbazones complexes on cell proliferation

The effect of new nickel (II) thiosemicarbazone complexes (**1**–**4**) on A549 cell line was determined by MTT. Cells were treated with

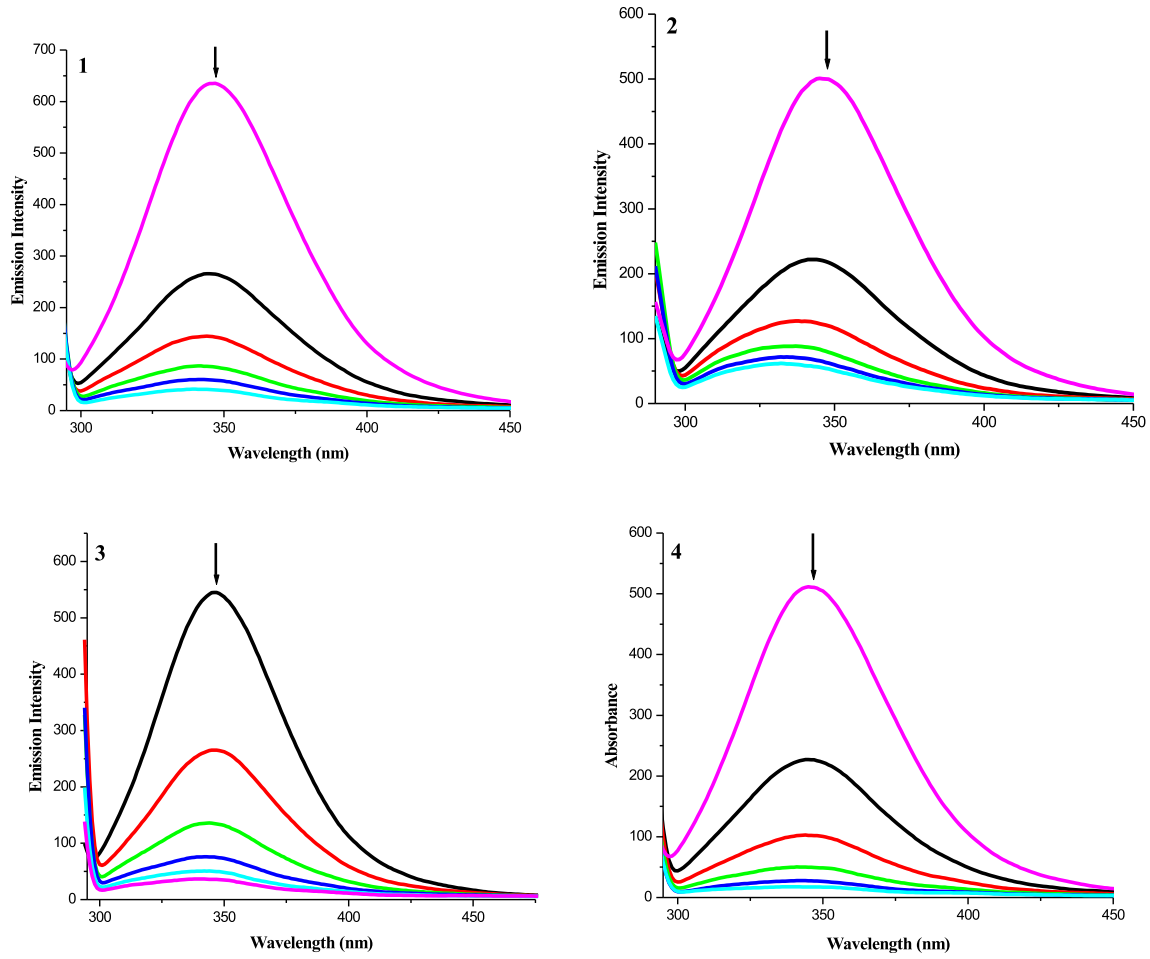

Fig. 6. The emission spectrum of BSA(1 μM; λ_{exc} = 280 nm; λ_{emi} = 346 nm) in the presence of increasing amounts of complexes **1**–**4** (0–25 μM). The arrow shows the emission intensity changes upon increasing complex concentration.

different concentrations (1–50 μM) of thiosemicarbazones for different time periods. No cytotoxicity was observed up to 10 μM concentration. The cell proliferation declined in a dose dependent manner when the cells were exposed to more than 10 μM for an incubation period of 12 and 24 h and there were no significant reduction in cell proliferation by the complexes when compared with control cells. In turn, the newly synthesized complexes significantly decreased the A549 cell proliferation with an exposure time of 48 h. Hence, we selected 48 h time period as optimum for the action of the nickel complexes used in the present study (Fig. 7). When the A549 cells were exposed to complexes (**1**–**4**) for 48 h the IC_{50} values were nearly 30 μM as shown in Table 5. Hence 15 and 30 μM concentrations were used for further studies. Among the four complexes, ethyl substituted thiosemicarbazone effectively declined the proliferation of lung adenocarcinoma cell line. [16c] Light microscopic analyses of the cells treated with nickel complexes showed significant morphological changes as shown in Fig. 8.

Table 4
Binding constant and number of binding sites for interaction of complexes with BSA.

System	K_b ($\times 10^7$ M^{-1})	n
BSA + 1	1.98	1.1971
BSA + 2	2.06	1.2151
BSA + 3	3.07	1.2388
BSA + 4	1.94	1.1929

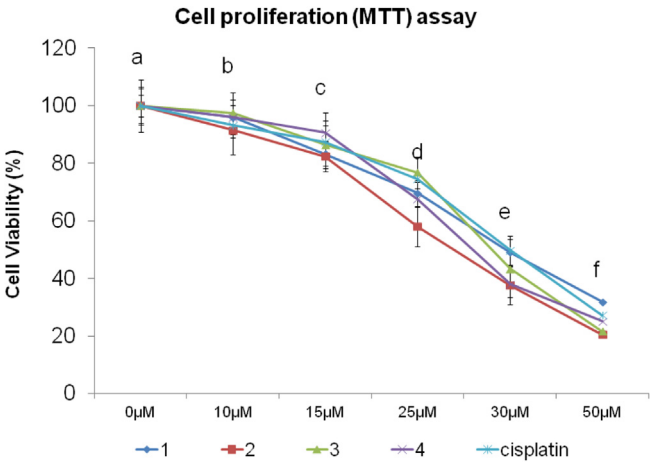

Fig. 7. The newly synthesized nickel complexes (**1**–**4**) inhibit A549 cell proliferation in a dose dependent manner. A549 cells were treated with different concentrations of complexes for 48 h, the cell viability was determined and the results were expressed as percentage cell viability with control. Results shown are mean ± SEM, which are three separate experiments performed in triplicate. Means not sharing a superscript letter differ significantly at $P < 0.05$ (One way ANOVA followed by Tukey's multiple comparison test).

Table 5
IC50 values of complexes **1**–**4**.

S. No.	complexes	IC_{50} (μm)
1.	**1**	29 ± 1.02
2.	**2**	30 ± 1.01
3.	**3**	27 ± 0.99
4.	**4**	28 ± 0.97
5.	**cisplatin**	25 ± 0.99

3.5.1. Cytotoxic effect of Ni(II) thiosemicarbazone on A549 cells

The cytotoxic effect of complexes **1**–**4** on A549 cell line was determined by Lactate dehydrogenase (LDH) leakage and nitric oxide release into the extracellular medium. Even though there are several cytotoxic enzyme markers are reported, their use has been limited by the presence of low amount in many cells and hence an elaborate kinetic assay is required to measure most enzyme activities. LDH is a stable cytoplasmic enzyme which is released into the culture medium following loss of membrane integrity resulting from apoptosis. LDH activity, therefore, can be used as an indicator of cell membrane integrity and serves as a general means to assess cytotoxicity resulting from chemical compounds or environmental toxic factors [91,92]. In the present study, significant level of LDH leakage was observed in the cell culture medium of A549 cell line, when the complexes were treated with two different concentrations for a period of 48 h. Complexes had the tendency to increase LDH leakage even at low dose such as 15 μM whereas LDH liberation after treatment with 30 μM concentration was highly significant in comparison with control indicating that the effect was dose dependent. Complex **3** showed significant level of LDH leakage in A549 cells compared to cisplatin. This authenticate that complex **3** was more effective than complex **1**, **2** and **4**.

NO plays an important role in many physiological processes including vascular regulation, immune responses and neural communication. Nitric Oxide (NO), produced endogenously from L-Arginine by the action of NO synthase (NOS), an enzyme existing in three isoforms. Among them, two isoforms exist constitutively and the third isoform is an inducible form (iNOS) which is expressed in response to stress. During oxidative stress, it has been shown that the expression of iNOS was increased which in turn leads to the nitric oxide accumulation. When excess, nitric oxide damages most of the biomolecules, including DNA and protein [93]. NO is extremely unstable and undergoes rapid oxidative degradation to the stable product nitrite (NO_2^-) which can be spectrophotometrically determined. The level nitric oxide release was significantly increased by the complexes **1**–**4** treated on lung adenocarcinoma cell line (A549) compared with control cells. Among them complex **3** is more effective in the induction of cytotoxicity in terms of both LDH and NO release in A549 cells (Fig. S18).

3.5.2. A549 cell migration inhibition studies by Ni(II) thiosemicarbazones

Metastatic cancers have several important characteristics, including the migratory and invasive activities of tumour cells. In order to examine the inhibitory effect of complexes **1**–**4** on cancer cell migration, A549 cells were incubated in the absence or presence of these complexes for wound migration assay. As shown in Fig. 9, complex treatment strongly suppressed A549 cell migration to the wounded area in a concentration-dependent manner. This indicates that the complexes could suppress the A549 cell migration, thereby metastasis.

3.5.3. Ni(II) thiosemicarbazones induced ROS hypergeneration and lipid peroxidation

Reactive oxygen species (ROS) is a term which encompasses all highly reactive, oxygen-containing molecules, including free radicals. The role of oxidative stress in vascular diseases, diabetes, renal

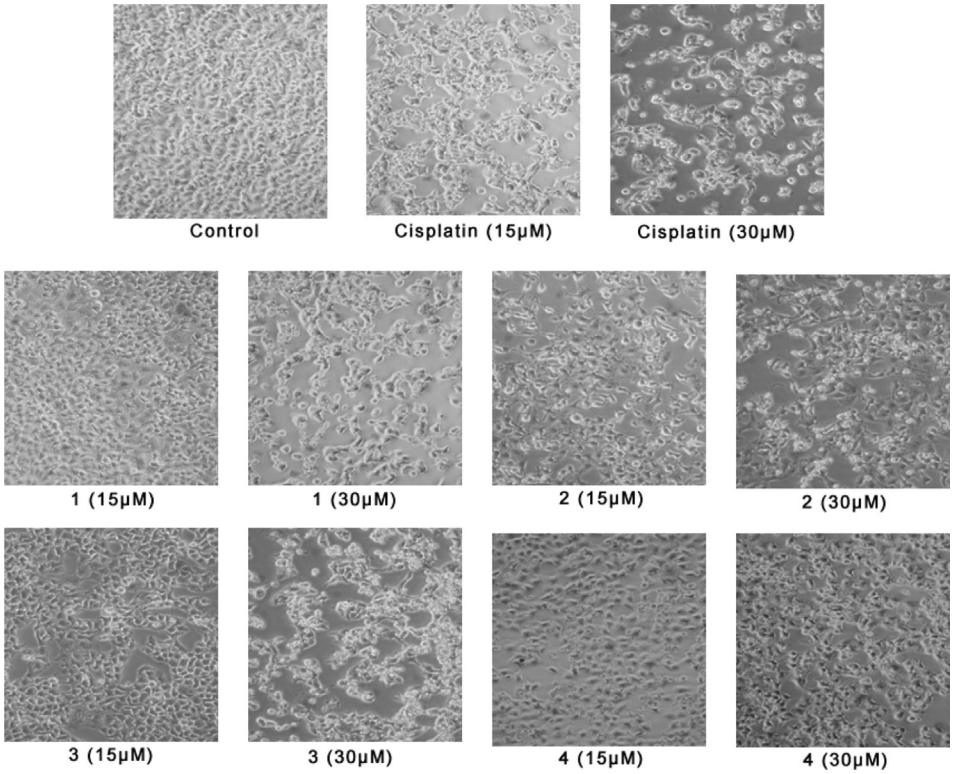

Fig. 8. Light microscopic analysis. Compared with control, remarkable morphologic changes of cells were observed in cells treated with complexes. These figures are representative of one experiment out of three with similar results.

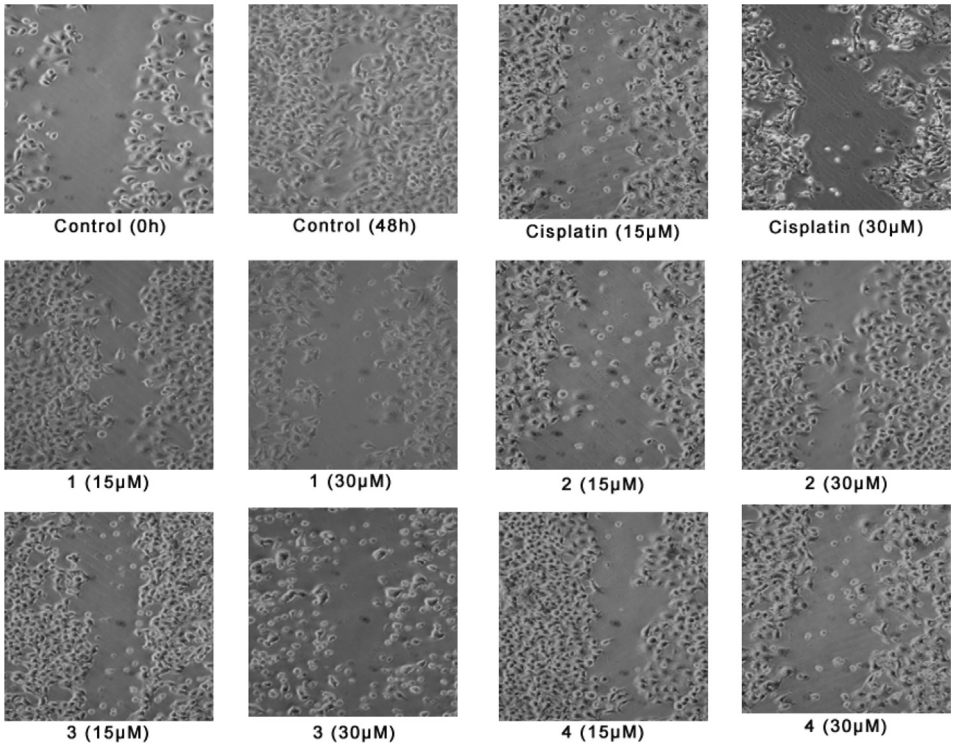

Fig. 9. Complexes **1**–**4** prevents A549 cell migration. After overnight attachment, a wound was created by scratching with a pipette tip and the cells were treated with complexes **1**–**4** for 48 h and light microscopic pictures were captured for observing cell migration. The four complexes strongly suppressed A549 cell migration to the wounded area in a concentration-dependent manner. These figures are representative of one experiment out of three with similar results.

ischaemia, atherosclerosis, pulmonary pathological states, inflammatory diseases, and cancer has been well established. ROS are highly reactive metabolites generated during normal cell metabolism; however, elevated intracellular ROS could be sufficient to trigger apoptosis [94,95]. Moreover, apoptotic cell death is reported to be preceded by the following sequential facts: ROS production, loss of mitochondrial trans-membrane potential, release of cytochrome C, and activation of caspase-3 [96]. To determine whether ROS are involved in complex induced apoptotic machinery, the level of ROS in the cells treated with the complexes **1**–**4** was measured. The ROS generation was determined for short time periods (15 min, 30 min and 1 h) since ROS production is an early event in apoptosis. The results demonstrate that the ROS generation was significantly increased within 15 min and peaked at 30 min (Fig. 10). With incubation period of 60 min there was decline in the ROS generation. Our results correlate with the finding of Pelosi et al. [97] in which thiosemicarbazone increased ROS generation in 41 M and SK-BR-3 cell lines. These results revealed the fact that nickel (II) complexes (**1**–**4**) mediate apoptosis by ROS hypergeneration. Ethyl substituted complex induced ROS hypergeneration more efficiently than the other substitutions.

It has been shown that lipid hydroperoxides and oxygenated products of lipid peroxidation can participate in the signal transduction cascade, control of cell proliferation and apoptosis [98].

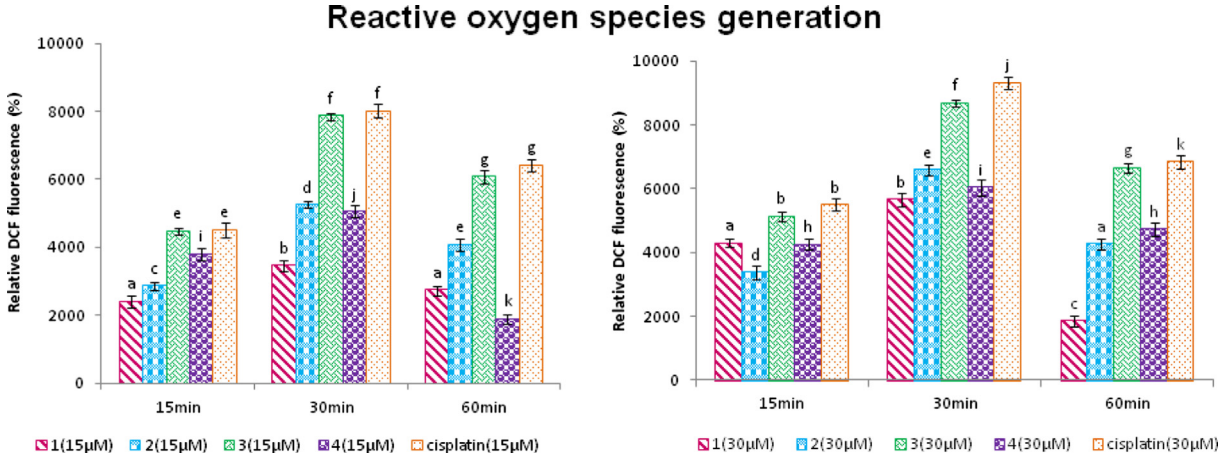

Fig. 10. Treatment of complexes **1**–**4** resulted in hypergeneration of intracellular reactive oxygen species (ROS). Intracellular ROS generation was evaluated at 15, 30 and 60 min after treatment with 15 μM and 30 μM Nickel (II) complexes **1**–**4** and the results were expressed as relative DCF fluorescence % of control. Statistical analysis showed a significant increase in ROS levels in cells treated with all four complexes as compared to control cells and it peaked with an exposure time of 30 min. Results shown are mean ± SEM, which are three separate experiments performed in triplicate. Means not sharing a superscript letter differ significantly at $P < 0.05$ (One way ANOVA followed by Tukey's multiple comparison test).

Table 6
Effect of nickel(II) complexes (**1**–**4**) on the activities of antioxidant enzymes: Activities of SOD, CAT, GPx, and GST, were evaluated in A549 cells treated with nickel(II) complexes for 48 h and the values were expressed as U/mg of protein. Activities of all the tested antioxidant enzymes were significantly reduced when compared with control cells.

U/mg of protein	SOD[a]		CAT[b]		GPx[c]		GST[d]	
	15 μM	30 μM	15 μM	30 Mm	15 μM	30 μM	15 μM	30 μM
Control	6543.33 ± 1.94^{P}		0.201 ± .00037^{P}		3395.86 ± 1.16^{P}		73.73 ± 0.32^{P}	
1	3886.54 ± 0.86^{e}	1587.08 ± 3.4^{E}	0.075 ± 0.01^{e}	0.060 ± 0.004^{E}	2442.9 ± 0.47^{e}	1573.84 ± 1.26^{E}	40.28 ± 0.51^{e}	29.79 ± 0.35^{E}
2	3380.95 ± 2.2^{f}	845.46 ± 1.78^{F}	0.097 ± .001^{f}	0.040 ± 0.01^{F}	2065.3 ± 1.6^{f}	1375.19 ± 1.56^{F}	43.68 ± 0.50^{f}	15.83 ± 0.28^{F}
3	1091.12 ± 6.2^{g}	748.54 ± 2.7^{G}	0.060 ± 0.01^{g}	0.031 ± 0.001^{G}	1751.2 ± 1.2^{g}	1260.12 ± 1.01^{G}	37.22 ± 0.35^{g}	13.23 ± 0.27^{G}
4	3380.2 ± 2.37^{h}	815.87 ± 1.31^{H}	0.083 ± .011^{h}	0.039 ± 0.002^{H}	2330.5 ± 1.9^{h}	1458.41 ± 0.57^{H}	62.03 ± 0.48^{h}	12.07 ± 0.33^{H}
Cisplatin	1195.78 ± 0.66^{i}	794.69 ± 0.86^{I}	0.063 ± 0.02^{i}	0.034 ± 0.01^{I}	1784.19 ± 0.62^{i}	1364.42 ± 0.66^{I}	39.93 ± 0.51^{i}	14.17 ± 0.42^{I}

[a] For SOD, 1U corresponds to the amount of enzyme required to give 50% inhibition of pyrogallol auto-oxidation.
[b] For CAT, 1U corresponds to the amount of enzyme that consumes 1 nmole H_2O_2/min.
[c] For GPx, 1U corresponds to the amount of enzyme that converts 1 μmole GSH to GSSG in the presence of H_2O_2/min.
[d] For GST, 1 U corresponds to the amount of enzyme that conjugates 1μmole CDNB/min. Results shown are Mean ± SEM, which are three separate experiments performed in triplicate. Means not sharing a superscript letter differ significantly at $P < 0.01$ (One way ANOVA followed by Tukey's multiple comparison test).

Hence we further examined the effect of the complexes on lipid peroxidation. Lipid peroxidation was significantly increased in lung cancer cell lines treated with complex **3** than other complexes (Fig. S19). The complex induced ROS hypergeneration might be the reason for the production of peroxide free radicals in the drug treated cancer cells compared with control cells. Level of lipid peroxidation by cisplatin was lower in A549 cells than the complexes.

3.5.4. Depletion of intracellular antioxidant pool by nickel(II) thiosemicarbazones

The presence of antioxidants in cells as a protective mechanism during oxidative stress and apoptotic cell death has been reported [99]. Oxidative stress indicates an imbalance state between production of ROS and antioxidant defenses. These defenses include superoxide dismutase, which converts O_2 to H_2O_2, glutathione peroxidase, and/or catalase, which in turn convert H_2O_2 to water. Antioxidants also play an important role against oxidant injury induced by an excess of ROS generation, by scavenging these species before they affect any biomolecules. An imbalance in these oxidant defenses leads to depletion of reduced glutathione (GSH), dissipation of mitochondrial transmembrane potential, lipid peroxidation, altered enzyme activities, DNA damage and eventual cell death by apoptosis [100]. Several earlier studies have demonstrated that the onset of apoptosis is associated with a fall of intracellular GSH in different cellular systems [101]. Hence we analysed the intracellular GSH content. The total reduced glutathione was significantly decreased in the cells exposed to complexes (**1**–**4**) with control cells (Fig. S20). Complex **3** effectively reduced the level of reduced glutathione in lung adenocarcinoma cells than the other complexes. In this study the enzymatic antioxidants such as SOD, CAT, GPx and GST were significantly decreased by

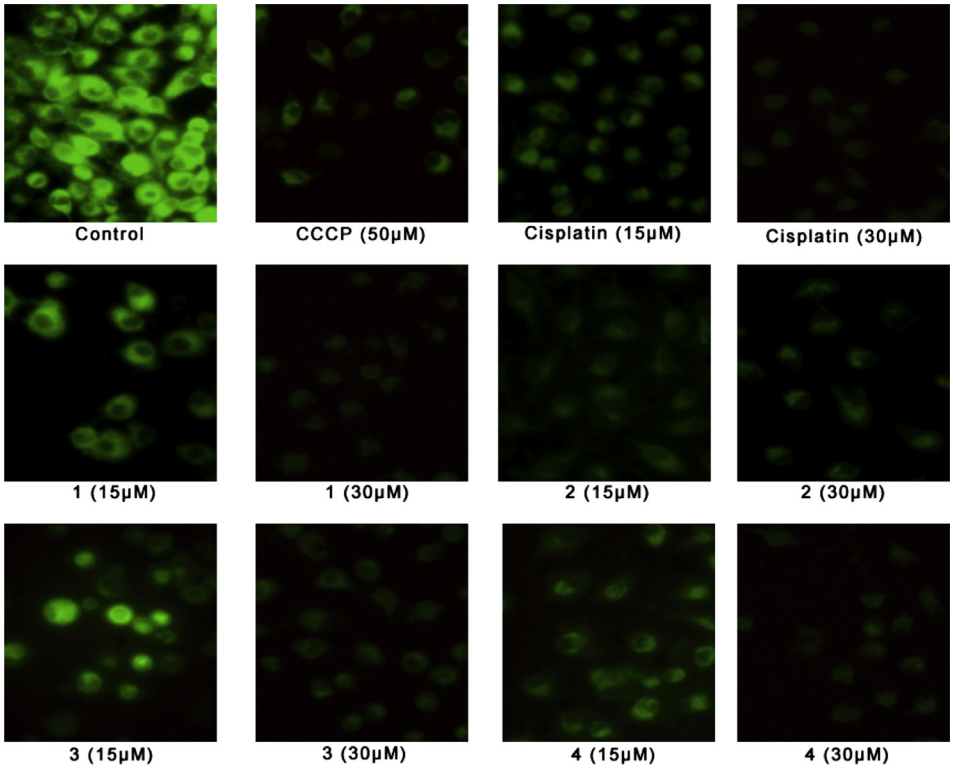

Fig. 11. Nickel(II) complexes **1**–**4** can dissipate mitochondrial membrane in A549 cells. Compared to control cells nickel(II) complexes **1**–**4** treated cells showed decrease in $DiOC_6$ fluorescence which is an indication of mitochondrial membrane damage. These figures are representative of one experiment out of three with similar results.

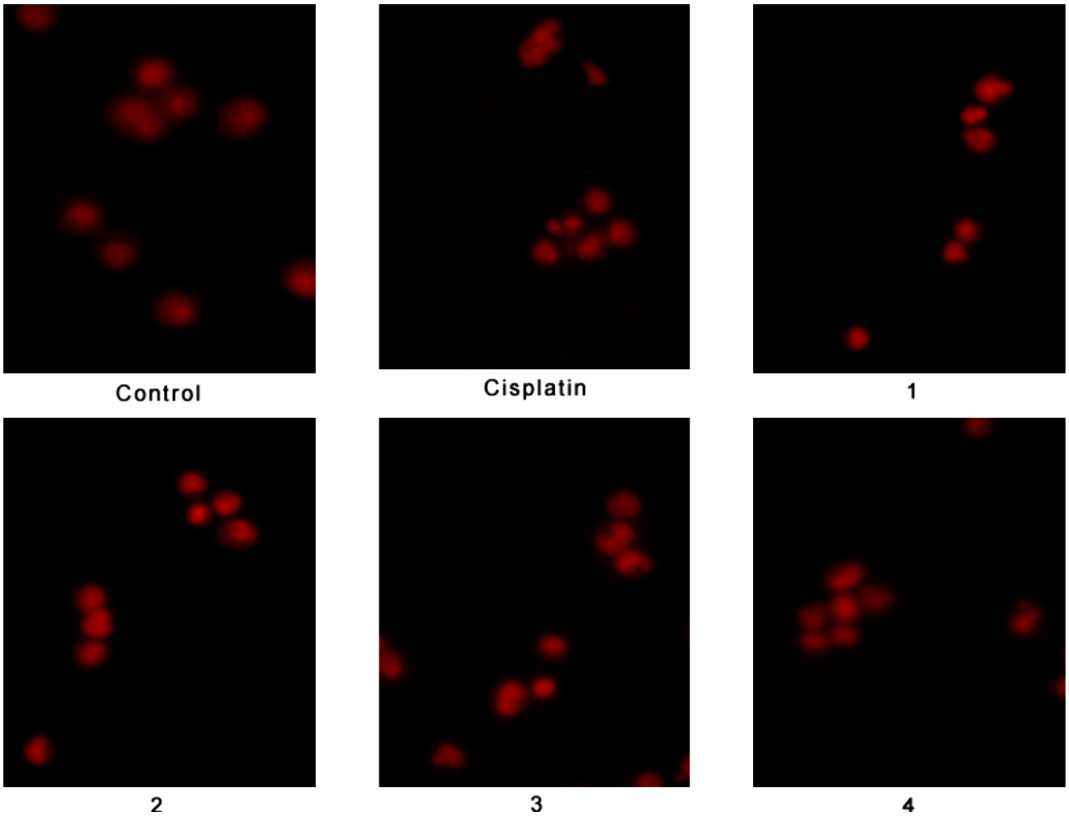

Fig. 12. Nickel(II) complexes **1**–**4** induce apoptosis in A549 cells. Apoptotic bodies were observed in nickel(II) complexes **1**–**4** treated human lung cancer cells (A549). Membrane blebbing indicates that these complexes are effective in inducing apoptosis. These figures are representative of one experiment out of three with similar results.

thiosemicarbazone treated A549 cancel cell line compared with control cells. Complex **3** is more effective than other complexes (Table 6). Even though the complexes could not deplete the antioxidant pool efficiently than cisplatin, however, exert their cytotoxic effect through the depletion of cellular antioxidant pool.

3.5.5. Mitochondrial membrane potential ($\Delta\psi M$) studies

The collapse of the mitochondrial transmembrane potential has been shown to promote (mitochondrial permeability transition) MPT. The MPT is a critical event in cell death following inhibition of the mitochondrial electron transport chain and is involved in the mechanism of mitochondrial dysfunction in apoptosis [102]. The MPT involves the formation of a non specific pore across the inner mitochondrial membrane, permitting the free distribution of ions, solutes, and small molecular weight molecules (1500 Da) across the membrane [103]. The opening of MPT induces the release of pro-apoptotic molecules, including AIF (apoptosis-inducing factor) and cytochrome C, from the intermembrane space in the cytoplasm [102]. Subsequently, cytochrome C interacts with Apaf-1, dATP/ATP, and procaspase-9 to form the apoptosome leading to activation of caspase-9 and downstream effector caspases [104]. The activated caspase 9 in turn activates the effector caspase 3 which on the other hand induces the apoptotic signalling cascade by activating ICAD.

To check whether the apoptosis induced by nickel complexes is through mitochondrial mediated pathway, $\Delta\psi M$ of the cells treated with nickel(II) complexes **1**–**4** was analysed. The results showed that the complexes are highly catastrophic to mitochondrial membrane and reduces the mitochondrial membrane potential as indicated by the decreased DiOC6 fluorescence in the cells treated with these complexes in comparison with control cells (Fig. 11). It is obvious from the results that these complexes **1**–**4** induces mitochondrial mediated apoptosis in human lung adenocarcinoma cell lines.

3.5.6. Nickel complexes induce apoptosis in lung adenocarcinoma cells

Cells die in response to a variety of stimuli and during apoptosis they do so in a controlled, regulated fashion. Cell death can be mediated through apoptosis or necrosis. Apoptosis is a type of programmed cell death and is now recognized as an important mode of cell death in response to cytotoxic treatments [105]. To check whether the complexes can induce apoptosis in lung adenocarcinoma cells, the propidium iodide staining was performed. Apoptotic cells can be distinguished from the normal cells by cell membrane blebbing which is the morphologic characteristic of apoptosis. Since the complexes showed a dose dependent activity in all the assays, the further studies were carried out using

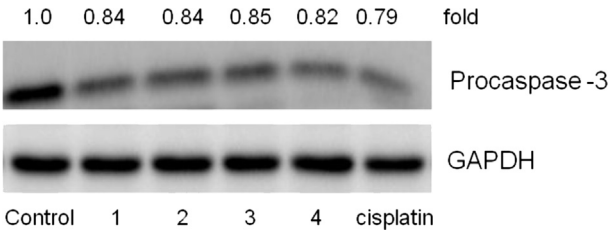

Fig. 13. Effect of Nickel(II) thiosemicarbazone complexes **1**–**4** on expression levels of procaspase 3. An equal amount of protein were electrophoresced and transferred on nitrocellulose membrane and the proteins were detected using specific antibodies as explained in materials and methods. GAPDH served as loading control. Nickel thiosemicarbazone complexes **1**–**4** could significantly reduce the expression levels of procaspase 3 thereby indicating their cleavage to caspase 3. These figures are one representative of three experiments with similar results.

only the higher concentration of the complexes (30 μM). As shown in Fig. 12 apoptotic bodies were visible in the cells treated with nickel(II) complexes **1**–**4**. These results confirm the apoptotic inducing nature of the thiosemicarbazone complexes.

Cleavage of nuclear DNA is regarded as a biochemical hallmark of apoptosis. DNA fragmentation is a key feature of programmed cell death, and the process is characterized by the activation of endogenous endonucleases with subsequent cleavage of chromatin DNA into internucleosomal fragments [106]. In normal cells, Caspase-activated deoxyribonuclease (CAD) binds with its specific inhibitor and form a complex called ICAD. During apoptosis, caspase-9 damages the nuclear pores in an unknown fashion so that activated caspase-3 can enter the nucleus to cleave ICAD. This releases the CAD from the complex, which can result in DNA degradation [107]. To further confirm the apoptotic induction by the complexes, procaspase 3 expression levels and DNA fragmentation analysis were also performed. From the results obtained it was obvious that the nickel(II) complexes containing-3-methoxysalicylaldehyde 4(*N*) substituted thiosemicarbazones induce apoptosis by reducing the levels of procaspase 3 which is an indication of activation of caspase 3 and fragmenting DNA molecule in the cell (Fig. 13 and Fig. S21). The extent of apoptosis induction was more with the higher concentration of the complexes.

4. Conclusion

New nickel(II) thiosemicarbazone complexes have been synthesized and characterized by various spectro and analytical techniques. The true nature of coordination of the ligand with the central metal atom was established by X-ray crystallographic studies. From the study, it is inferred that in complex **1**, the ligand coordinated as tridentate monobasic nature and the remaining complexes the ligands coordinated as tridentate bibasic nature. In order to know about their potential binding ability of the new complexes, CT-DNA and BSA protein were taken as models. The complexes bind to CT-DNA through intercalation mode and with BSA, the quenching was found as static. Taken together our data entertain the notion that the newly synthesized nickel complexes induce cytotoxicity in human lung cancer cells (A549) via LDH and NO release into the culture medium. The complexes could encourage ROS hyper-generation with subsequent depletion of intracellular antioxidant pool and mitochondrial membrane depolarization leading to caspase activation and DNA fragmentation which were the hallmarks of apoptosis. Thus the complexes could induce mitochondrial mediated apoptosis. From all the above studies, it is clearly evident that complex **3** exhibited higher activity than all other complexes. In addition, the present investigation lights up the antimetastatic effect of nickel complexes by inhibiting A549 cell migration. Hence, further studies on animal models to elucidate the clear mechanism of action of the complexes are highly warranted to unveil the nickel complexes as anticancer drugs.

Acknowledgement

The authors gratefully acknowledge Council of Science and Industrial research (CSIR), New Delhi, India and Department of Science and Technology (DST), New Delhi, India for the financial support.

Appendix A. Supplementary material

Crystallographic data for [Ni(Msal-tsc)(PPh_3)].Cl (1) [Ni(MSal-mtsc)(PPh_3)] (2) and [Ni(Msal-ptsc)(PPh_3)] (4) have been deposited at the Cambridge Crystallographic Data Centre as supplementary publication (CCDC No. 958106, 958104 and 958105). The data can be obtained free of charge at www.ccdc.cam.ac.uk/conts/retrieving.html or from the Cambridge Crystallographic Data Centre, 12, Union Road, Cambridge CB2 1EZ, UK [fax: +44-1223/336-033; e-mail: deposit@ccdc.cam.ac.uk].

Appendix B. Supplementary material

Supplementary data associated with this article can be found in the online version, at http://dx.doi.org/10.1016/j.ejmech.2014.05.075.

References

[1] World Health Organization. Cancer, fact sheet no. 297Æ http://www.who.int/mediacentre/factsheets/fs297/en/æ (accessed February 2012).
[2] G. Tonon, K.K. Wong, G. Maulik, C. Brennan, B. Feng, Y. Zhang, D.B. Khatry, A. Protopopov, M.J. You, A.J. Aguirre, E.S. Martin, Z. Yang, H. Ji, L. Chin, R.A. Depinho, High-resolution genomic profiles of human lung cancer, Proc. Natl. Acad. Sci. U. S. A. 102 (2005) 9625–9630.
[3] S. Padhye, Z. Afrasiabi, E. Sinn, J. Fok, K. Mehta, N. Rath, Antitumor metallothiosemicarbazonates: structure and antitumor activity of palladium complex of phenanthrenequinone thiosemicarbazone, Inorg. Chem. 44 (2005) 1154–1156.
[4] P.J. Barnard, B.S.J. Price, Targeting the mitochondrial cell death pathway with gold compounds, Coord. Chem. Rev. 251 (2007) 1889–1902.
[5] N.J. Wheate, S. Walker, G.E. Craig, R. Oun, The status of platinum anticancer drugs in the clinic and in clinical trials, Dalt. Trans. 39 (2010) 8113–8127.
[6] E. Wong, C.M. Giandomenico, Current status of platinum-based antitumor drugs, Chem. Rev. 99 (1999) 2451–2466.
[7] Z. Guo, P.J. Sadler, Metals in medicine, Angew. Chem. Int. Ed. 38 (1999) 1512–1531.
[8] M.S. Razzaque, Cisplatin nephropathy: is cytotoxicity avoidable? Nephrol. Dial. Transpl. 22 (2007) 2112–2116.
[9] M. Okuda, K. Masaki, S. Fukatsu, Y. Hashimoto, K. Inui, Role of apoptosis in cisplatin-induced toxicity in the renal epithelial cell line LLC-PK1. Implication of the functions of apical membranes, Biochem. Pharmacol. 59 (2000) 195–205.
[10] K. van der Schilden, F. García, H. Kooijman, A.L. Spek, J.G. Haasnoot, J. Reedijk, A highly flexible dinuclear ruthenium(II)-platinum(II) complex: crystal structure and binding to 9-ethylguanine, Angew. Chem. Int. Ed. 43 (2004) 5668–5670.
[11] J.M. Pérez, V. Cerrillo, A.I. Matesanz, J.M. Millán, P. Navarro, C. Alonso, P. Souza, DNA interstrand cross-linking efficiency and cytotoxic activity of novel cadmium(II)–thiocarbodiazone complexes, ChemBioChem 2 (2001) 119–123.
[12] T.W. Hambley, The influence of structure on the activity and toxicity of Pt anti-cancer drugs, Coord. Chem. Rev. 166 (1997) 181–223.
[13] J. Kasparkova, V. Marini, Y. Najajreh, D. Gibson, V. Brabec, DNA binding mode of the cis and trans geometries of new antitumor nonclassical platinum complexes containing piperidine, piperazine, or 4-picoline ligand in cell-free media. Relations to their activity in cancer cell lines, Biochemistry 42 (2003) 6321–6332.
[14] M. Huxley, C. Sanchez-Cano, M.J. Browning, C. Navarro-Ranninger, A.G. Quiroga, A. Rodger, M.J. Hannon, An androgenic steroid delivery vector that imparts activity to a non-conventional platinum(II) metallo-drug, Dalt. Trans. 39 (2010) 11353–11364.
[15] S. Leininger, B. Olenyuk, P.J. Stang, Self-assembly of discrete cyclic nanostructures mediated by transition metals, Chem. Rev. 100 (2000) 853–908.
[16] S. Feng, R. Xu, New materials in hydrothermal synthesis, Acc. Chem. Res. 34 (2001) 239–247.
[17] M. Yuan, Y. Li, E. Wang, J. Chem. Soc. Dalt. Trans. 4 (2002) 2916.
[18] Y. Lu, E. Wang, M. Yuan, Hydrothermal synthesis and crystal structure of a layered vanadium phosphate with a directly coordinated organonitrogen ligand: [$V_4O_7(HPO_4)_2$(2,2′-bipy)$_2$], J. Chem. Soc. Dalt. Trans. 15 (2002) 3029–3031.
[19] B. Maity, S. Gadadhar, T.K. Goswami, A.A. Karande, A.R. Chakravarty, Photoinduced anticancer activity of polypyridyl platinum(II) complexes, Eur. J. Med. Chem. 57 (2012) 250–258.
[20] R. Loganathan, S. Ramakrishnan, E. Suresh, A. Riyasdeen, M. Abdulkadhar, M.A. Akbarsha, M. Palaniandavar, Mixed ligand copper(II) complexes of *N*,*N*-bis(benzimidazol-2-ylmethyl)amine (BBA) with diimine co-ligands: efficient chemical nuclease and protease activities and cytotoxicity, Inorg. Chem. 51 (2012) 5512–5532.
[21] K.E. Erkkila, D.T. Odom, J.K. Barton, Recognition and reaction of metallointercalators with DNA, Chem. Rev. 99 (1999) 2777–2796.
[22] B. Meunier, Metalloporphyrins as versatile catalysts for hydrocarbon oxygenations and oxidative DNA cleavage, Chem. Rev. 92 (1992) 1411–1456.
[23] G. Pratviel, J. Bernadou, B. Meunier, Carbon—hydrogen bonds of DNA sugar units as targets for chemical nucleases and drugs, Angew. Chem. Int. Ed. 34 (1995) 746–769.

[24] D.S. Sigman, A. Mazumder, D.M. Perrin, Chemical nucleases, Chem. Rev. 93 (1993) 2295–2316.
[25] J. Reedijk, New types of antitumor compounds and their interaction with nucleic acids, J. Inorg. Biochem 86 (2001) 89.
[26] C.J. Burrows, J.G. Muller, Oxidative nucleobase modifications leading to strand scission, Chem. Rev. 98 (1998) 1109–1152.
[27] K.J. Duffy, A.N. Shaw, E. Delorme, S.B. Dillon, C. Erickson-Miller, L. Giampa, Y. Huang, R.M. Keenan, P. Lamb, N. Liu, S.G. Miller, A.T. Price, J. Rosen, H. Smith, K.J. Wiggall, L. Zhang, J.I. Luengo, Identification of a pharmacophore for thrombopoietic activity of small, non-peptidyl molecules 1. Discovery and optimization of salicylaldehyde thiosemicarbazone thrombopoietin mimics, J. Med. Chem. 45 (2002) 3573–3575.
[28] J.R. Dilworth, R. Hueting, Metal complexes of thiosemicarbazones for imaging and therapy, Inorg. Chim. Acta 389 (2012) 3–15.
[29] J.A. Lessa, I.C. Mendes, P.R.O. da Silva, M.A. Soares, R.G. dos Santos, N.L. Spezialic, N.C. Romeiro, E.J. Barreiro, H. Beraldo, 2-Acetylpyridine thiosemicarbazones: cytotoxic activity in nanomolar doses against malignant gliomas, Eur. J. Med. Chem. 45 (2010) 5671–5677.
[30] R.J. Glisoni, M.L. Cuestas, V.L. Mathet, J.R. Oubina, A.G. Moglioni, A. Sosnik, Antiviral activity against the hepatitis C virus (HCV) of 1-indanone thiosemicarbazones and their inclusion complexes with hydroxypropyl-β-cyclodextrin, Eur.J. Pharm. Sci. 47 (2012) 596–603.
[31] X. Du, C. Guo, E. Hansel, P.S. Doyle, C.R. Caffrey, T.P. Holler, J.H. McKerrow, F.E. Cohen, Synthesis and structure–activity relationship study of potent trypanocidal thio semicarbazone inhibitors of the trypanosomal cysteine protease cruzain, J. Med. Chem. 45 (2002) 2695–2707.
[32] D. Kovala-Demertzi, M.A. Demertzis, E. Filiou, A.A. Pantazaki, P.N. Yadav, J.R. Miller, Y. Zheng, D.A. Kyriakidis, Platinum(II) and palladium(II) complexes with 2-acetyl pyridine 4N-ethyl thiosemicarbazone able to overcome the cis-platin resistance. Structure, antibacterial activity and DNA strand breakage, Biometals 16 (2003) 411–418.
[33] J.P. Scovill, D.L. Klayman, D.G. Franchino, 2-Acetylpyridine thiosemicarbazones. 4. Complexes with transition metals as antimalarial and antileukemic agents, J. Med. Chem. 25 (1982) 1261–1264.
[34] L. Klayman, J.P. Scovill, J.F. Bartosevich, J. Bruce, 2-Acetylpyridine thiosemicarbazones. 5. 1-[1-(2-Pyridyl)ethyl]-3-thiosemicarbazides as potential antimalarial agents, J. Med. Chem. 26 (1983) 35–39.
[35] D.K. Demertzi, M.A. Demertzis, J.R. Miller, C. Papadopoulou, C. Dodorou, G. Filousis, Platinum(II) complexes with 2-acetyl pyridine thiosemicarbazone: synthesis, crystal structure, spectral properties, antimicrobial and antitumour activity, J. Inorg. Biochem 86 (2001) 555–563.
[36] P.K. Singh, D.N. Kumar, Spectral studies on cobalt(II), nickel(II) and copper(II) complexes of naphthaldehyde substituted aroylhydrazones, Spectrochim. Acta A 64 (2006) 853–858.
[37] J.C. Cymerman, D. Wills, S.D. Rubbo, J. Edgar, Mode of action of *iso* nicotinic hydrazide, Nature 176 (1955) 34–35.
[38] S. Padhye, G.B. Kaufman, Transition metal complexes of semicarbazones and thiosemicarbazones, Coord. Chem. Rev. 63 (1985) 127–160.
[39] M.J.M. Campbell, Transition metal complexes of thiosemicarbazide and thiosemicarbazones, Coord. Chem. Rev. 15 (1975) 279–319.
[40] S.K. Chattopadhyay, M. Hossain, A.K. Guha, S. Ghosh, Ligational behaviour of two biologically active N– S donors towards cobalt (III), iron (III), iron (II) and rhodium (III), Transit. Met. Chem. 15 (1990) 473–477.
[41] G.J. Palenik, D.F. Rendle, W.S. Carter, The crystal and molecular structures of thiosemicarbazones; an antitumor agent 5-hydroxy-2-formylpyridine thiosemicarbazone sesquihydrate and the inactive acetone thiosemicarbazone, Acta Crystallogr. Sect. B 30 (1974) 2390–2395.
[42] H.J. Kruger, R.H. Holm, Stabilization of trivalent nickel in tetragonal NiS4N2 and NiN6 environments: synthesis, structures, redox potentials and observations related to [NiFe]-hydrogenases, J. Am. Chem. Soc. 112 (1990) 2955–2963.
[43] Z. Lu, C. White, A.L. Rheingold, R.H. Crabtree, Deprotonated thioamides as thiolate S-donor ligands with a high tendency to avoid M-S-M bridge formation: crystal and molecular structure of bis(2-hydroxy-5-methylacetophenone N,N-dimethylthiosemicarbazonato)dinickel, Inorg. Chem. 32 (1993) 3991–3994.
[44] S. Mandal, P.K. Bharadwaj, Z.Y. Zhou, T.C.W. Mak, A hexadentate nickel(II) complex with a tripodal ligand bearing S_3N_3donors: synthesis, spectroscopic and X-ray crystal structural investigation, Polyhedron 14 (1995) 919–926.
[45] G.J. Colpas, M. Kumar, R.O. Day, M.J. Maroney, Structural investigations of nickel complexes with nitrogen and sulfur donor ligands, Inorg. Chem. 29 (1990) 4779–4788.
[46] S.B. Choudhury, D. Ray, A. Chakravorty, Nickel(III)-sulfur binding. Chemistry of the tris(xanthate) family, Inorg. Chem. 29 (1990) 4603–4611.
[47] S.W. Ragsdale, H.G. Wood, J.A. Morton, L.G. Ljungdahl, D.V. Dervartanian, in: J.R. Lancaster Jr. (Ed.), The Bioinorganic Chemistry of Nickel, VCH, New York, Chapter 14, 1988.
[48] G. Pelosi, Thiosemicarbazone metal complexes: from structure to activity, Open. Crystallogr. J. 3 (2010) 16–28.
[49] M. Frezza, S.S. Hindo, D. Tomco, M.M. Allard, Q.C. Cui, M.J. Heeg, D. Chen, Q.P. Dou, C.N. Verani, Comparative activities of nickel(II) and zinc(II) complexes of asymmetric [NN′O] ligands as 26S proteasome inhibitors, Inorg. Chem. 48 (2009) 5928–5937.
[50] T. Chattopadhyay, M. Mukherjee, A. Mondal, P. Maiti, A. Banerjee, K.S. Banu, S. Bhattacharya, B. Roy, D.J. Chattopadhyay, T.K. Mondal, M. Nethaji, E. Zangrando, D. Das, A unique nickel system having versatile catalytic activity of biological significance, Inorg. Chem. 49 (2010) 3121–3129.
[51] R. Prabhakaran, P. Kalaivani, R. Huang, P. Poornima, V. Vijaya Padma, F. Dallemer, K. Natarajan, DNA binding, antioxidant, cytotoxicity (MTT, lactate dehydrogenase, NO), and cellular uptake studies of structurally different nickel(II) thiosemicarbazone complexes: synthesis, spectroscopy, electrochemistry, and X-ray crystallography, J. Biol. Inorg. Chem. 18 (2013) 233–247.
[52] R. Prabhakaran, P. Kalaivani, P. Poornima, F. Dallemer, G. Paramaguru, V. Vijaya Padma, R. Renganathan, K. Natarajan, One pot synthesis of structurally different mono and dimeric Ni(II) thiosemicarbazone complexes and N-arylation on a coordinated ligand: a comparative biological study, Dalt. Trans. 41 (2012) 9323–9336.
[53] P. Kalaivani, R. Prabhakaran, E. Ramachandran, F. Dallemer, G. Paramaguru, R. Renganathan, P. Poornima, V. Vijaya Padma, K. Natarajan, Influence of terminal substitution on structural, DNA, protein binding, anticancer and antibacterial activities of palladium(II) complexes containing 3-methoxy salicylaldehyde-4(N) substituted thiosemicarbazones, Dalt. Trans. 41 (2012) 2486–2499.
[54] P. Kalaivani, R. Prabhakaran, F. Dallemer, P. Poornima, E. Vaishnavi, E. Ramachandran, V. Vijaya Padma, R. Renganathan, K. Natarajan, DNA, protein binding, cytotoxicity, cellular uptake and antibacterial activities of new palladium(II) complexes of thiosemicarbazone ligands: effects of substitution on biological activity, Metallomics 4 (2012) 101–113.
[55] S. Purohit, A.P. Koley, L.S. Prasad, P.T. Manoharan, S. Ghosh, Chemistry of molybdenum with hard-soft donor ligands. 2.' Molybdenum(VI), -(V), and -(IV) oxo complexes with tridentate schiff base ligands, Inorg. Chem. 28 (1989) 3735–3742.
[56] J. Venanzi, Tetrahedral nickel(II) complexes and the factors determining their formation. Part I. Bistriphenylphosphine nickel(II) compounds, J. Chem. Soc. 43 (1958) 719–724.
[57] A.I. Vogel, Textbook of Practical Organic Chemistry, fifth ed., vol. 268, Longman, London, 1989.
[58] R.H. Blessing, Data reduction and error analysis for accurate single crystal diffraction intensities, Crystallogr. Rev. 1 (1987) 3–58.
[59] R.H. Blessing, DREADD – data reduction and error analysis for single-crystal diffractometer data, J. Appl. Crystallogr. 22 (1989) 396–397.
[60] R.H. Blessing, An empirical correction for absorption anisotropy, Acta Crystallogr. Sect. A: Found. Crystallogr. A51 (1995) 33–38.
[61] G.M. Sheldrick, SHELXTL Version 5.1, An Integrated System for Solving, Refining and Displaying Crystal Structures from Diffraction Data, Siemens Analytical X-ray Instruments, Madison, WI, 1990.
[62] G.M. Sheldrick, SHELXL-97, Program for Refinement of Crystal Structures, University of Göttingen, Germany, 1997.
[63] M. Tim, Rapid colorimetric assay for cellular growth and survival: application to proliferation and cytotoxicity assays, J. Immunol. Methods 65 (1983) 55–63.
[64] D.D. Ulmer, B.L. Vallee, W.E. Wacker, Metalloenzymes and myocardial infarction. II. Malic and lactic dehydrogenase activities and zinc concentrations in serum, N. Engl. J. Med. 255 (1956) 450–456.
[65] D.J. Stuehr, M.A. Marletta, Synthesis of nitrite and nitrate in murine macrophage cell lines, Cancer Res. 47 (1987) 5590–5594.
[66] C.P. LeBel, H. Ischiropoulos, S.C. Bondy, Evaluation of the probe 2',7'-dichlorofluorescin as an indicator of reactive oxygen species formation and oxidative stress, Chem. Res. Toxicol. 5 (2) (1992) 227–231.
[67] O.H. Lowry, N.J. Rosebrough, A.L. Farr, R.J. Randall, Protein measurement with the Folin phenol reagent, J. Biol. Chem. 193 (1951) 265–275.
[68] G. Pereira-Caro, R. Mateos, B. Sarria, R. Cert, L. Goya, L. Bravo, Hydroxytyrosyl acetate contributes to the protective effects against oxidative stress of virgin olive oil, Food Chem. 131 (2012) 869–878.
[69] S. Marklund, G. Marklund, Involvement of the superoxide anion radical in the autoxidation of pyrogallol and a convenient assay for superoxide dismutase, Eur. J. Biochem. 47 (1974) 469–474.
[70] H. Aebi, Methods of Enzymatic Analysis, Academic Press, New York (, 1974.
[71] W.H. Habig, M.J. Pabst, W.B. Jakoby, Glutathione S-transferases. The first enzymatic step in mercapturic acid formation, J. Biol. Chem. 249 (1974) 7130–7139.
[72] J.T. Rotruck, A.L. Pope, H.E. Ganther, A.B. Swanson, D.G. Hafeman, W.G. Hoekstra, Selenium: biochemical role as a component of glutathione peroxidase, Science 179 (1973) 588–590.
[73] J. Gong, F. Traganos, Z.A. Darzynkiewicz, A selective procedure for DNA extraction from apoptotic cells applicable for gel electrophoresis and flow cytometry, Anal. Biochem. 218 (1994) 314–319.
[74] R. Prabhakaran, P. Kalaivani, R. Huang, M. Sieger, W. Kaim, P. Viswanathamurthi, F. Dallemer, K. Natarajan, Can geometry control the coordination behaviour of 2-hydroxy-1-naphthaldehyde-N(4)-phenyl-thiosemicarbazone? A study towards its origin, Inorg. Chim. Acta 376 (2011) 317–324.
[75] R. Prabhakaran, C. Jayabalakrishnan, V. Krishnan, K. Pasumpon, D. Sukanya, H. Bertagnolli, K. Natarajan, Preparation, spectral characterization, electrochemistry,EXAFS, antibacterial and catalytic activity of new ruthenium (III) complexes containing ONS donor ligands with triphenylphosphine/arsine, Appl. Organomet. Chem. 20 (2006) 203–213.
[76] R. Prabhakaran, S.V. Renukadevi, R. Karvembu, R. Huang, J. Mautz, G. Huttner, R. Subash kumar, K. Natarajan, Structural and biological studies of

mononuclear palladium(II) complexes containing N-substituted thiosemicarbazones, Eur. J. Med. Chem. 43 (2008) 268–273.
[77] R. Prabhakaran, R. Karvembu, S.V. Renukadevi, R. Huang, M. Zeller, K. Natarajan, Coordination behaviour of ferrocenylthiosemicarbazone in a novel hetero trinuclear nickel(II) complex: synthesis, spectral, electrochemistry and X-ray crystallography, Inorg. Chim. Acta 361 (2008) 2547–2552.
[78] J.G. Tojal, J.L. Dizarro, A.G. Orad, A.R. P-Sanz, M. Ugalda, A.A. Diaz, J.L. Serra, M.I. Arriortua, T. Rojo, Biological activity of complexes derived from thiophene-2-carbaldehyde thiosemicarbazone. Crystal structure of [Ni(C(6)H(6)N(3)S(2))(2)], J. Inorg. Biochem 86 (2001) 627–633.
[79] A.D. Naik, S.M. Annigeri, V.B. Gangadharmath, V.K. Revankar, V.B. Mahale, Structural diversity in dinickel(II) complexes of thiosemicarbazones, J. Mol. Struct. 616 (2002) 119.
[80] C. Rodrigues, A.A. Batista, R.Q. Aucélio, L.R. Teixeira, L.C. Visentin, H. Beraldo, Spectral and electrochemical studies of ruthenium(II) complexes with N^4-methyl-4-nitrobenzaldehyde and N^4-methyl-4-nitrobenzophenone thiosemicarbazone: potential anti-trypanosomal agents, Polyhedron 27 (2008) 3061–3066.
[81] R. Prabhakaran, R. Karvembu, T. Hashimoto, K. Shimizu, K. Natarajan, Formation of structurally different solvated and non-solvated [Ni(PTSC)(PPh_3)] (PTSC = salicylaldehyde-N-phenylthiosemicarbazide anion) crystals from single pot, Inorg. Chim. Acta 358 (2005) 2093–2096.
[82] P. Kalaivani, R. Prabhakaran, P. Poornima, F. Dallemer, K. Vijayalakshmi, V. Vijaya Padma, K. Natarajan, Versatile coordination behavior of salicylaldehydethiosemicarbazone in ruthenium(II) carbonyl complexes: synthesis, spectral, x-ray, electrochemistry, DNA binding, cytotoxicity, and cellular uptake studies, Organometallics 31 (2012) 8323–8332.
[83] A. Wolfe, G.H. Shimer, T. Meehan, Polycyclic aromatic hydrocarbons physically intercalate into duplex regions of denatured DNA, Biochemistry 26 (1987) 6392–6396.
[84] G. Cohen, H. Eisenberg, Viscosity and sedimentation study of sonicated DNA–proflavine complexes, Biopolymers 8 (1969) 45–55.
[85] Y.Z. Zhang, H.R. Li, J. Dai, W.J. Chen, J. Zhang, Y. Liu, Spectroscopic studies on the binding of cobalt(II) 1,10-phenanthroline complex to bovine serum albumin, Biol. Trace Elem. Res. 135 (2010) 136–152.
[86] R.M. Wang, J.J. Mao, J.F. Song, C.X. Huo, Y.F. He, Antioxidant activity of bovine serum albumin binding amino acid Schiff-bases metal complexes, Chin. Chem. Lett. 18 (2007) 1416–1418.
[87] H.Y. Liu, Z.H. Xu, X.H. Liu, P.X. Xi, Z.Z. Zeng, Analysis of binding interaction between bovine serum albumin and the cobalt(II) complex with salicylaldehyde-2-phenylquinoline-4-carboylhydrazone, Chem. Pharm. Bull. 57 (2009) 1237–1242.
[88] Y. Wang, H. Zhang, G. Zhang, W. Tao, S. Tang, Interaction of the flavonoid hesperidin with bovine serum albumin: a fluorescence quenching study, J. Lumin. 126 (2007) 211–218.
[89] M. Jiang, M.X. Xie, D. Zheng, Y. Liu, X.Y. Li, X. Chen, Spectroscopic studies on the interaction of cinnamic acid and its hydroxyl derivatives with human serum albumin, J. Mol. Struct. 692 (2004) 71–80.
[90] N. Wang, L. Ye, B.Q. Zhao, J.X. Yu, Spectroscopic studies on the interaction of efonidipine with bovine serum albumin, Braz. J. Med. Biol. Res. 41 (2008) 589–595.
[91] E. Bonfoco, D. Krainc, M. Ankarcrona, P. Nicotera, S.A. Lipton, Apoptosis and necrosis: two distinct events induced, respectively, by mild and intense insults with N-methyl-D-aspartate or nitric oxide/superoxide in cortical cell cultures, Proc. Natl. Acad. Sci. U. S. A. 92 (1995) 7162–7166.
[92] C. Legrand, J.M. Bour, C. Jacob, J. Capiaumont, A. Martial, A. Marc, M. Wudtke, G. Kretzmer, C. Demangel, D. Duval, Lactate dehydrogenase (LDH) activity of the cultured eukaryotic cells as marker of the number of dead cells in the medium, J. Biotechnol. 25 (1992) 231–243.
[93] L. Yu, P.E. Gengaro, M. Niederberger, T.J. Burke, R.W. Schrier, Nitric oxide: a mediator in rat tubular hypoxia/reoxygenation injury, Proc. Natl. Acad. Sci. 91 (1994) 1691–1695.
[94] J.F. Curtin, M. Donovan, T.G. Cotter, Regulation and measurement of oxidative stress in apoptosis, J. Immunol. Methods 265 (2002) 49–72.
[95] J. Chandra, A. Samali, S. Orrenius, Triggering and modulation of apoptosis by oxidative stress, Free Radic. Biol. Med. 29 (2000) 323–333.
[96] B. Herrera, M. Fernandez, A.M. Alvarez, C. Roncero, M. Benito, J. Gil, I. Fabregat, Activation of caspases occurs downstream from radical oxygen species production, Bcl-xL down-regulation, and early cytochrome C release in apoptosis induced by transforming growth factor beta in rat fetal hepatocytes, Hepatology 34 (2001) 548–556.
[97] G. Pelosi, F. Bisceglie, F. Bignami, P. Ronzi, P. Schiavone, M. Carla Re, C. Casoli, E. Pilotti, Antiretroviral activity of thiosemicarbazone metal complexes, J. Med. Chem. 53 (2010) 8765–8769.
[98] P. Cejas, E. Casado, C. Belda-Iniesta, J. De Castro, E. Espinosa, A. Redondo, M. Sereno, M.A. Garcia-Cabezas, J.A. Vara, A. Dominguez-Caceres, R. Perona, M. Gonzalez-Baron, Implications of oxidative stress and cell membrane lipid peroxidation in human cancer (Spain), Cancer Causes Control CCC 15 (2004) 707–719.
[99] C.S. Sharma, S. Sarkar, A. Periyakaruppan, J. Barr, K. Wise, R. Thomas, B.L. Wilson, G.T. Ramesn, Single-walled carbon nanotubes induces oxidative stress in rat lung epithelial cells, J. Nanosci. Nanotechnol. 7 (2007) 2466–2472.
[100] T. Panaretakis, I.G. Shabalina, D. Grander, M.C. Shoshan, J.W. DePierre, Reactive oxygen species and mitochondria mediate the induction of apoptosis in human hepatoma HepG2 cells by the rodent peroxisome proliferator and hepatocarcinogen, perfluorooctanoic acid, Toxicol. Appl. Pharmacol. 173 (2001) 56–64.
[101] A.G. Hall, Review: the role of glutathione in the regulation of apoptosis, Eur. J. Clin. Investig. 29 (1999) 238–245.
[102] M. Loeffler, G. Kroemer, The mitochondrion in cell death control: certainties and incognita, Exp. Cell. Res. 256 (2000) 19–26.
[103] P. Bernardi, K.M. Broekemeier, D.R. Pfeitfer, Recent progress on regulation of the mitochondrial permeability transition pore; a cyclosporin-sensitive pore in the inner mitochondrial membrane, J. Bioenerg. Biomembr. 26 (1994) 509–517.
[104] P. Li, D. Nijhawan, I. Budihardjo, S.M. Srinivasula, M. Ahmad, E.S. Alnemri, X. Wang, Cytochrome c and dATP-dependent formation of Apaf-1/Caspase-9 complex initiates an apoptotic protease cascade, Cell 91 (1997) 479–489.
[105] J.F. Kerr, C.M. Winterford, B.V. Harmon, Apoptosis. Its significance in cancer and cancer therapy, Cancer 73 (1994) 2013–2026.
[106] S. Baluchamy, P. Ravichandran, A. Periyakaruppan, V. Ramesh, J.C. Hall, Y. Zhang, O. Jejelowo, D.S. Gridley, H. Wu, G.T. Ramesh, Induction of cell death through alteration of oxidants and antioxidants in lung epithelial cells exposed to high energy protons, J. Biol. Chem. 285 (2010) 24769–24774.
[107] T.J. Fan, L.H. Han, R.S. Cong, J. Liang, Caspase family proteases and apoptosis, Acta Biochim. Biophys. 37 (2005) 719–727.